Environmental Science Nano

Accepted Manuscript

ROYAL SOCIETY OF CHEMISTRY

rsc.li/es-nano

Physical, Chemical, and *In Vitro* Toxicological Characterization of Nanoparticles in Chemical Mechanical Planarization Suspensions Used in the Semiconductor Industry: Towards Environmental Health and Safety Assessments

David Speed [1], Paul Westerhoff [2*], Reyes Sierra-Alvarez [3], Rockford Draper [4], Paul Pantano [4], Shyam Aravamudhan [5], Kai Loon Chen [6], Kiril Hristovski [2], Pierre Herckes [2], Xiangyu Bi [2], Yu Yang [2], Chao Zeng [3], Lila Otero-Gonzalez [3], Carole Mikoryak [4], Blake A. Wilson [4], Karshak Kosaraju [5], Mubin Tarannum [5], Steven Crawford [5], Peng Yi [6,9], Xitong Liu [6], S.V. Babu [7], Mansour Moinpour [8], James Ranville [10], Manuel Montano [10], Charlie Corredor [11], Jonathan Posner [11], and Farhang Shadman [3]

* Indicates corresponding author: Paul Westerhoff, Arizona State University, School of Sustainable Engineering & The Built Environment, PO Box 873005, Tempe, AZ 85287-3005; phone: 480-965-2885; email: p.westerhoff@asu.edu

[1] IBM Microelectronics, Systems and Technology Group (Hopewell Jct., NY)
[2] Arizona State University (Tempe, AZ)
[3] University of Arizona (Tucson, AZ)
[4] University of Texas at Dallas (Richardson, TX)
[5] North Carolina A&T State University (Greensboro, North Carolina)
[6] Johns Hopkins University (Baltimore, MD)
[7] Clarkson University (Potsdam, NY)
[8] Intel Corporation (Santa Clara, CA)
[9] Current address: Department of Civil, Environmental and Geomatics Engineering, Florida Atlantic University, Boca Raton, Florida 33431
[10] Colorado School of Mines (Golden, CO)
[11] University of Washington (Seattle, WA)

In preparation for submission to *Environmental Science: Nano*

keywords: nanomaterial, toxicity, analysis, wastewater

Abstract

This tutorial review focuses on aqueous slurries of dispersed engineered nanoparticles (ENPs) used in chemical mechanical planarization (CMP) for polishing wafers during manufacturing of semiconductors. A research consortium was assembled to procure and conduct physical, chemical, and *in vitro* toxicity characterization of four ENPs used in CMP. Based on input from experts in semiconductor manufacturing, slurries containing fumed silica (*f*-SiO_2), colloidal silica (*c*-SiO_2), ceria (CeO_2), and alumina (Al_2O_3) were selected and subsequently obtained from a commercial CMP vendor to represent realistic ENPs in simplified CMP fluids absent of proprietary stabilizers, oxidants, or other chemical additives that are known to be toxic. ENPs were stable in suspension for months, had highly positive or negative zeta potentials at their slurry working pH, and had mean diameters measured by dynamic light scattering (DLS) of 46±1 nm for *c*-SiO_2, 148±5 nm for *f*-SiO_2, 132±1 nm for CeO_2, and 129±2 nm for Al_2O_3, all of which were larger than the sub 100 nm diameter primary particle sizes measured by electron microscopy. The concentration of ENPs in all four slurries that caused 50% inhibition (IC-50) was greater than 1 mg/mL based on *in vitro* assays using bioluminescence of the bacterium *Aliivibrio fischeri* and the proliferation, viability, and integrity of human cells (adenocarcinomic human alveolar basal epithelial cell line A549). The general practice in the CMP industry is to dilute the slurry waste stream so actual abrasive concentrations are typically orders of magnitude smaller than 1 mg/mL, which is lower than IC-50 levels. In contrast to recent reports, we observed similar toxicological characteristics between *c*-SiO_2 and *f*-SiO_2, and the materials exhibited similar X-ray diffraction (XRD) spectra but different morphology observed using electron microscopy. The ENPs and CMP slurries used in this study have been made available to a number of other research groups, and it is the intention of the consortium for this paper to provide a basis for characterizing and understanding human and environmental exposures for this important class of industrial ENPs.

1. Introduction

Some industrial processes use large quantities of engineered nanoparticles (ENPs) in ways that do not directly end up in consumer products but which nonetheless require appropriate handling and environmental controls to assure that they do not pose workplace and/or environmental risks. The provision of effective and safe handling methods, and the provision of effective waste treatment and disposal methods requires knowledge of how ENP behave in air and aqueous matrices, as well as the availability of well informed human and ecotoxicity threshold values. The ability to establish these factors is in turn predicated on the availability of validated analytical methods for the quantification of ENP in relevant air, water and solid media. Efforts to evaluate ENP behavior in environmental systems face difficult metrology challenges [6, 7]. In particular, there is a need for validated methodologies that can discriminate between dissolved and nano-sized particulates, measure particle number and size distributions, and differentiate between ENPs and naturally occurring nanoparticles.

Alumina (Al_2O_3), ceria (CeO_2), and silica (SiO_2) represent an important class of ENPs[1]. One principal use of Al_2O_3, CeO_2, and amorphous SiO_2 nanoparticles is chemical mechanical planarization (CMP) where particles in the form of abrasive slurries are used to polish wafers when fabricating integrated circuits in the semiconductor industry [17, 18]. In this application, the ENPs are used to manufacture the product (semiconductor chips), but are not incorporated into the product. CMP nanoparticles constituted nearly 60% of the total $1 billion worldwide market for nano-powders in 2005 [19, 20].

Although Al_2O_3, CeO_2, and amorphous SiO_2 ENP are generally believed to be relatively innocuous, toxicity evaluations that have been conducted on these materials, vary depending on the particular aspects of the particles being assessed (e.g., particle size, physiochemical properties, and dispersion state) as well as the particular toxicity assessment method being utilized (e.g., dose, cell lines, exposure protocols, and assay end points) [2, 3]. Likewise, there is some uncertainty regarding the behavior and fate of these ENP in wastewater treatment processes. For instance, the removal of CeO_2, SiO_2, and Al_2O_3 nanopartcles (NPs) during biological wastewater treatment has received some research attention [8-14], but less information

exists on ENP removal in the type of physical-chemical treatment processes that are often employed as on-site industrial wastewater treatment. The available literature indicates that Al_2O_3 and CeO_2, but not necessarily SiO_2, are typically removed well by conventional biological wastewater treatment processes. ENPs removed from the wastewater accumulate in biosolids and precipitated sludges, where their fate and ultimate stability are important considerations when determining the environmental effects of these ENPs. Moreover, naturally occurring Al_2O_3 and SiO_2 NPs are believed to be common in natural water systems, where their fate intertwined with a variety of geological and biological processes [15, 16]. An understanding of the background concentrations and geochemical processes that govern the occurrence and behavior of these naturally occurring NPs, and how biota respond to them, is needed to provide context for interpreting the impacts of ENP wastewater discharges and determining appropriate discharge levels. In light of these information gaps, we have pursued a multi-university collaborative research effort, the initial stages of which have centered on developing and validating basic characterization methods for Al_2O_3, CeO_2, and amorphous SiO_2.

This tutorial review aims to characterize ENPs in model CMP suspensions, to understand the ramifications of ENP properties on potential exposure and toxicity to environmental systems and humans, and to discuss research needs associated with the next generation of semiconductor manufacturing. Four model CMP fluids, each being the simplest formulation to generate a stable suspension of ENPs, were obtained from a major commercial slurry manufacturer. These slurries were thoroughly characterized via physical-chemical means, including intra-laboratory comparisons of nano-measurements. Large volumes of these model CMP suspensions were procured and have been made available to several investigators that study workplace exposure, human and ecosystem toxicity, industrial treatment efficiencies, sewer discharge and wastewater treatment removal, fate and transport, and fundamental aspects of the nano-bio interface. *In vitro* assays were conducted using different cell lines to compare the relative toxicity of ENPs used in CMP. Finally, a discussion identifies potential scenarios for workplace exposure and flux of ENPs from CMP processes into the sewer system.

1.1. Nanoparticle Use in Semiconductor Production

Al_2O_3, CeO_2, and amorphous SiO_2 ENPs are used in a variety of applications beyond CMP [1]. For example, Al_2O_3 is used in the production of tires, paper, catalyst, polymers, and personal care products; CeO_2 is used in fuel additives, catalyst, and biomedical applications; and SiO_2 is used in the manufacture of tires, paper, paints, coatings, catalyst, cement, polymers, and personal care products. Annual production volume of Al_2O_3, CeO_2, and SiO_2 has been estimated and presented in a number of recent publications but varies widely, as indicated in Table 1.

CMP fluids remove materials by a combination of chemical and mechanical (or abrasive) actions to achieve highly smooth and planar material surfaces. CMP, which can be used to planarize a variety of materials including dielectrics, semiconductors, metals, polymers, and composites, is one of the most important semiconductor processes for achieving the performance goals of modern microprocessor and memory chips [21, 22]. Fig. 1 shows a typical CMP operation scheme where a robotic arm loads a semiconductor wafer onto a rotating plate, a quantity of CMP slurry is dispensed, and a pad is engaged in a polishing action that uses the slurry to planarize the wafer surface. The polishing step is followed by additional automated rinse and pad cleaning steps. Following the CMP operation, the height of the wafer surface is typically uniform to within ±1 nm, or less. Because even the smallest scratch or surface imperfection can ruin the geometry of the integrated circuit being fabricated into a wafer, CMP slurries are typically crafted with highly controlled particle size distributions, along with additives, as described below.

The inorganic oxide abrasive particles are an important constituent for CMP slurries, with the three most commonly used abrasive particles being Al_2O_3, amorphous SiO_2, and CeO_2 [17, 23]. Depending on the particular application, particle size in CMP slurries can vary from 20 to 200 nm, and trends are toward CMP particles < 100 nm in size to achieve highly polished surfaces [23, 24]. In a given slurry formulation, these particles usually have a uniform shape and size.

Amorphous SiO_2 can be distinguished as fumed silica (*f*-SiO_2) and colloidal SiO_2 (*c*-SiO_2) based on the synthesis methods. *f*-SiO_2 is formed in a pyrogenic process by oxidizing chlorosilane ($SiCl_4$) at high temperature [25]. *c*-SiO_2 is formed in liquid phase by precipitating a Si precursor (e.g., Na_2SiO_3) [26]. A widely referenced method of synthesizing *c*-SiO_2 that uses a tetraalkyl silicate as the Si precursor was presented by Stöber [27]. CeO_2 NPs used in CMP slurries have a crystalline structure, thus often yielding sharp edges, corners, and apexes [28]. Al_2O_3 NPs

used in CMP slurries can be α-Al_2O_3, ß-Al_2O_3, δ-Al_2O_3, or fumed Al_2O_3 [29]. Al_2O_3 is softer than SiO_2 or CeO_2 and sometimes can be coated with a hard surface such as SiO_2 to enhance semi-conductor polishing [23].

In addition to the metal oxide NPs, CMP slurries may also contain a number of additives, such as pH adjustment agents, oxidizers, dispersants, complexing agents, surfactants, biocides, and corrosion inhibitors, as summarized in Table 2. For instance, one additive may serve to aid in the selective dissolution and solubilization of a material that is present at the wafer surface, and a second additive may serve to protect or inhibit the removal of a different material that is present on the exposed wafer surface during the CMP process. Likewise, surface active agents may be added to influence particle surface charge and help maintain a stable particle dispersion.

In a manufacturing line, a combination of CMP slurries is fed to a fleet of CMP tools. In each tool, the wafers undergo the CMP process and are rinsed with deionized (DI) water, and further chemicals may be added to clean and/or recondition the wafer polishing pads. A typical wafer production step might involve applying between 0.2 and 0.8 L of CMP slurry, 1 to 2 L of rinse water, and another 5 or more liters of pad cleaner and rinse water. The total quantity of wastewater generated per wafer undergoing CMP polishing may be on the order of 10 or more liters. The effluent wastewater contains the original slurries, associated rinse waters, and dissolved and particulate material that is removed from the wafer during the CMP operation. The thickness of material removed from the wafer surface may vary from a few nanometers to 100 or more nanometers. If, for instance, a 100 nm blanket layer of Cu is removed from a 300 mm diameter wafer surface, 64 mg Cu/wafer would be added to the wastewater.

Detailed characterization of the compositional change that a CMP slurry undergoes throughout a given CMP process has not been reported in the literature. However, there are reports that the particle size distribution in CMP waste is typically broader than the particle size distribution of the virgin slurry [30, 31], which is probably due to the release of small particles from the wafer surface, the formation of aggregates, or both.

2. Analytical & Experimental Methods

2.1. CMP Fluid Procurement

Through an industry-university collaboration supported by the Semiconductor Research Corporation (SRC) and the SRC Engineering Research Center for Environmentally Benign Semiconductor Manufacturing, our consortium was able to work with a CMP slurry provider (Cabot Inc.) to design and procure large volumes of four fairly simple, industrially relevant, and well characterized CMP slurries. Because the slurries were custom synthesized, there were no intellectual property challenges to overcome nor any proprietary chemical additives. Table 3 summarizes the physiochemical properties of the four CMP slurries, including information provided by the manufacturer (shown in the top row). Acidic *c*-SiO_2 was prepared in acetic acid while *f*-SiO_2 was in a basic solution of KOH. The CeO_2 slurry was provided without any additives. According to supplier, the cerium oxide is made from a high temperature (>300 C) calcination process followed by milling/re-sizing, and based upon our industrial authors the majority of commercially available ceria slurries used in the silica wafer processing industry use calcined ceria. The Al_2O_3 slurry was provided in dilute nitric acid. CMP NPs were dispersed using a common industry method involving a high-energy dispersion machine [32].

2.2. Particle Sizing and Zeta Potential Analysis

Particle sizing was conducted using Brookhaven ZetaPALS or Bl-200SM and Malvern ZS ZEN3600 instruments, different laser wavelengths (659, 488, 633 nm), and different scattering angles (90°, 90°, 173°). Refractive indexes were 1.765 for Al_2O_3, 2.200 for CeO_2, and 1.542 for SiO_2. The electrophoretic mobilities (EPMs) of the slurries were measured using either the Malvern Zetasizer Nano ZS ZEN3600 or the Brookhaven ZetaPALS Analyzer. The EPMs of the slurries were then converted into zeta (ζ) potentials using the Smoluchowski equation[33]. Slurries were prepared for both measurements using either DI water or 10 mM ionic strength solutions (adjusted with either NaCl or $NaHCO_3$), and the EPM measurements were conducted over a broad range of pH conditions (3–11).

Nanoparticle Tracking Analysis (NTA) was performed using a NanoSight LM10 instrument (NanoSight Ltd., Amesbury, United Kingdom) equipped with a 405 nm (blue) laser source, a temperature-controlled chamber, and a scientific CMOS camera (Hamamatsu). A video (30 s) of each sample was collected and analyzed using NTA 2.3 Build 011 software (NanoSight Ltd.). The concentration (particles per mL) was calculated as the average of three replicates.

Single particle ICP-MS (spICP-MS) is an emerging nano-analysis to size and quantify NPs in liquid matrices [34-36]. An ICP-MS instrument (Perkin-Elmer NexION 300q) was placed in time-resolved analysis mode in which the signal was recorded every dwell time (integration time of one reading by the detector) of 10 ms. Thus, the detection of a particle gave a pulse signal. The sample flow rate was 0.6–0.7 mL/min. Si^{29}, ^{140}Ce, and ^{27}Al were used as the analyte isotopes for SiO_2, CeO_2, and Al_2O_3 NPs.

2.3. Chemical Digestion and Analysis of CMP Nanoparticles

All NPs were digested using a microwave-assisted system and a suitable digestion mixture. Tetramethylammonium hydroxide (4 mL of TMAH, 25%) was used to digest SiO_2 NPs samples (11 mL). For CeO_2 and Al_2O_3, 2 mL HF (50%), 2 mL HCl (30%, J. T. Baker), and 6 mL HNO_3 (70%) were added to the sample, and the total volume was adjusted to 15-20 mL. The microwave was operated as follows: ramping to 150°C in 15 min; next ramping to 180°C in 15 min; and holding at 180°C for 30 min. Metals were analyzed using an ICP-MS (Thermo X series II ICP-MS).

2.4. Separation of Nanoparticles from Dissolved Ions

Two methods were employed and compared to separate NPs from dissolved ions. First, a centrifugal ultrafiltration device (Millipore, Darmstadt, Germany), which combines an ultrafiltration (UF, 30 kDa nominal molecular weight limit) membrane and a centrifuge tube, was adopted as a tool to separate NPs and the ionic species (liquid phase). Samples in the centrifugal UF devices (10 mL) were centrifuged at 5000 ×g for 30 min. To demonstrate the effectiveness of the centrifugal UF device to separate NPs and dissolved species, a commercial SiO_2 nanoparticle (PM1040, Nissan Chemical, Houston) and an ionic SiO_2 standard solution (HACH, Loveland) were used. Three samples containing: 1) 1000 µg/L (as SiO_2) ionic standard and 1000 µg/L (as SiO_2) NPs; 2) 1000 µg/L NPs; and 3) 1000 µg/L ionic standard were tested in triplicate. The recoveries of filtrate and concentrate for all cases were ≥ 94%. In the second method, slurries were centrifuged in a two-step procedure to remove NPs and provide supernatants for analysis. Slurry aliquots (1.5 mL) were centrifuged at 20,000 ×g for 60 min, and 1.2 mL of the supernatant was collected. Subsequently, the supernatant was centrifuged at 100,000 ×g for 60 min.

242

243 **2.5. Anions and Dissolved Organic Carbon**

244 Acetate was monitored using an Agilent 7890A gas chromatography system (Agilent
245 Technologies, Santa Clara, CA, USA) fitted with a Restek Stabilwax-DA column (30 m x 0.35
246 mm, ID 0.25 μm) and a flame ionization detector. Nitrate was analyzed by suppressed
247 conductivity – ion chromatography using a Dionex IC-3000 system (Sunnyvale, CA, USA) fitted
248 with a Dionex IonPac AS11 analytical column (4 mm x 250 mm) and an AG11 guard column (4
249 mm x 40 mm). The flow rate was 1 mL/min, and run time was 10 min per sample. An isocratic
250 mobile phase containing 30 mM KOH was employed. The dissolved organic carbon (DOC) was
251 determined using a Shimadzu TOC-500A total organic carbon analyzer (Shimadzu Scientific
252 Instruments, Columbia, MD, USA).

253

254 **2.6. Solid State Characterization**

255 Scanning electron microscopy systems equipped with an energy dispersive X-ray microanalysis
256 system (SEM/EDX) (FEG ESEM Philips XL30 with EDAX system) and high-resolution
257 transmission electron microscopy systems (HR-TEM) coupled with energy dispersive X-ray
258 spectroscopy (EDX) (Philips CM200 FEG HR-TEM/STEM) were used. X-ray diffraction was
259 performed using an Agilent-Gemini X-Ray diffractometer with a molybdenum source in a
260 Bragg–Brentano arrangement. All slurries were dried to a constant mass at 125ºC prior to
261 analysis. The Fourier transform infrared spectroscopy (FTIR) analysis was performed in an
262 attenuated total reflectance (ATR) spectrophotometer (Varian 600 FT-IR) in the range of 400-
263 4000 cm^{-1} at a resolution of 1 cm^{-1}.

264

265 **2.7 CMPs Catalytic Activity Analysis**

266 The catalytic activity of CMPs (*c*-SiO_2 and *f*-SiO_2) using our Colorimetric Assay to Detect
267 Engineered nanoparticles (CADE) technique described elsewhere in detail [37]. Briefly, CADE
268 employs a dye, methylene blue (MB), and a reducing agent, sodium borohydride (BH_4), to
269 colorimetrically assess the catalytic activity of nanoparticles in an aqueous media (see SI for
270 more information).

2.8. *In Vitro* Assays

In vitro assays were conducted using marine bacterium *Aliivibrio fischeri* (MicroTox® Bioasssay) and adenocarcinomic human alveolar basal epithelial cells (A549 cell viability, ATCC® CCL-185™). The dye 3-(4,5-dimethylthiazol-2-yl)-2,5-diphenyltetrazolium bromide (MTT) assay kit (Sigma Aldrich) was used to quantitatively evaluate the cell viability of A549 cells after exposure to the CMP slurries, and the Lactate dehydrogenase (LDH) kit (Sigma Aldrich) was used to evaluate the membrane integrity of A549 cells. Proliferation of A549 cells was measured by two methods: determination of cell numbers by staining nucleic acids with crystal violet dye (CV), or direct counting of cell numbers with a Coulter counter. Details of these methods are provided in Supplemental Information.

3. Results

3.1. Chemical Composition of Nanoparticles and CMP Slurries

The “model slurries" employed in the initial phase of this work represent the simplest possible stable dispersion of particles in water. As such, they contrast with the complexity of commercial CMP slurries that are formulated with a wide variety of ingredients, including a number of chemicals that are known to be toxic on their own and surface active and redox active chemicals (Table 2) that are intended to influence particle behavior. Bulk primary metal concentrations in the as-received slurries ranged from 9.6 to 50 g/L and agreed with the manufacturer reported data of 1 to 5% (Table 3). Digested slurries were analyzed for additional elements (Fig. 2) to quantify the presence of impurities, especially elements potentially toxic to cells. Each slurry contained different ratios of trace elements relative to the primary CMP NP. Fig. 2 presents the concentrations of elements in the slurry that were detected at concentrations above laboratory blanks. Calcium and zinc were detected as impurities in all the samples at levels of 10 to 100 mg/L, which is roughly 1000 times lower than the primary metal elements (Si, Ce, or Al) that were present in the slurry at 9.6 to 50 g/L. The SiO_2-based slurries contained aluminum at 1 to 20 mg/L and titanium, iron, and small amounts of either gold, magnesium, and/or copper at concentrations below 5 mg/L. The high concentration of potassium in the *f*-SiO_2 slurry is

associated with addition of KOH (Table 1). The Al_2O_3 slurry contained less than 1 mg/L iron, magnesium, titanium, zirconium, copper, and chromium. The CeO_2 slurry contained the largest number of detectable elements, including hafnium, palladium, silver, and gold, which may have been co-occurring elements residual from the mining and separation process. Likewise, impurities in the feedstocks for SiO_2 and Al_2O_3 probably cause impurities in the slurries and could possibly be used as unique markers for tracing the fate of CMP NPs in the environment as has been attempted for other types of NPs (e.g., TiO_2 NPs from sunscreens into rivers [38]). Analysis of metals was performed at two different universities, and comparable results were obtained.

In order to differentiate elements associated with the CMP particles from elements dissolved in solution, supernatants after high-speed centrifugation or permeates of 30kDA ultrafilters were analyzed (Fig. 3). Both preparation methods yielded very similar concentrations, thus validating their use in laboratories that may only have access to one method (Fig. 3). In general, the same elements detected in the digested, as-received slurry were also detectable in the NP-free solutions. In all cases, the concentrations of all detectable elements in the aqueous aliquots of the slurries were far below levels detected in the as-received digested slurry, and most trace elements were below 1000 µg/L. This suggests that the NPs partially dissolved and released ionic forms of these elements. Whereas levels of zinc were high in some CMP slurry NPs (Fig. 2), they were much lower in free solution (Fig. 3). The as-received slurries were diluted many fold prior to toxicity testing (discussed in section 3.5), and the predicted effect of dissolved zinc was below levels of concern for toxicity. Elevated levels of potassium in the *f*-SiO_2 slurry and supernatant were notable but expected because the slurry was adjusted to basic pH with KOH (Table 3).

Three of the slurries had low levels of dissolved organic carbon (1.9 to 6.7 mg/L), but the *c*-SiO_2 dispersion had much higher DOC (320 mg/L) because high levels of acetic acid were present (~800 mg/L) (Table 3). Nitrate was detected (135 mg NO_3^-/L) in the Al_2O_3 slurry that contained nitric acid. Both the acetic acid and nitrate were associated with pH control agents added to adjust pH to levels where the NPs should be stable in suspension (discussed in section 3.4).

3.2. Solid-State Analysis of Nanoparticles

XRD spectra of the NPs in the CMP slurries were obtained to characterize their crystalline nature and purity (Fig. 4). The two SiO_2 samples gave similar spectra, showing a broad halo in XRD pattern, clearly indicating an amorphous SiO_2 structure. The CeO_2 slurry shows strong peaks at (111), (200), and (220) for CeO_2 that are consistent with literature [39]. The Al_2O_3 slurry shows a strong peak at (111) and weaker peaks at (311) and (400), as observed elsewhere [40].

Fig. 5 shows FTIR analysis of the slurries. Broad stretching around 3000–3500 cm^{-1} is attributed to OH stretch from water, and the peak around 1650 cm^{-1} is attributed to C=C stretching and indicates the presence of organic contaminants in the slurries. Colloidal and fumed SiO_2 showed a band around 1120 cm^{-1} corresponding to asymmetric stretching vibration of Si-O-Si band [41] in which the bridging oxygen atom moves parallel to the Si-Si lines in the opposite direction to their Si neighbors and a second band around ~470 cm^{-1} corresponding to Si-O rocking vibration where the oxygen atom moves perpendicular to the Si-O-Si plane. FTIR spectra for the other two slurries show Ce-O and Al-O stretching in the region of 500-750 cm^{-1} [39, 40].

Differentiating forms of silica is important to the semiconductor industry which uses both fumed and colloidal silica for CMP operations. Fumed silica has been used since CMP processes were first developed in the 1980s and provides a comparatively inexpensive and rapid means of planarizing oxide surfaces. However, it is stable only at alkaline pH and generally provides a lower quality surface than colloidal silica, which became available in the 1990s. Fumed silica particles are normally multi-fractal, irregularly shaped with sharp edges and surfaces and is produced via high temperature combustion of $SiCl_4$ with oxygen, whereas colloidal silica, made via a sol-gel process using either water glass (Na or K silicates) or tetramethoxysilane (TMOS) and tetraethoxysilane (TEOS), is available in the form of uniform spherical particles over a wide range of pH and size distributions and is generally used where a highly smooth surface is required. Despite very different uses by industry, it can be difficult to differentiate *f*-SiO_2 from *c*-SiO_2 using common solid-state characterization methods. However, literature incorporating nuclear magnetic resonance analysis suggests that the surface hydroxyl concentration and formation of bi-nuclear surface complexes with metals in solution reacting with the SiO_2

surfaces (i.e., proximity of surface group) are perhaps more important than the morphological structure [42, 43].

3.3. Shape and Size Characterization

Table 3 summarizes CMP NP sizing information and shows sizing of primary particles via electron microscopy differs from measurements of the NPs in dispersions where aggregates are present.

Fig. 6 shows imaging and sizing results using electron microscopy. The *c*-SiO_2 NPs are nearly spherical, compared with more angular and rectangular shaped CeO_2 NPs. The *f*-SiO_2 NPs appeared fused together to an extent not apparent with SiO_2. The angular shape and non-spherical morphology of three of the four NPs was initially unexpected because CMP NPs are routinely described as nearly spherical polishing agents. However, the non-spherical nature of some CMP NPs influences their ability to scratch surfaces being polished [44]. The Al_2O_3 NPs appeared to be aggregates of smaller primary particles having a broad range of diameters. Using both TEM and SEM images, the particle size distributions of the shortest dimension of the NPs were made (Fig. 6 and Table 3). The primary particles in the two SiO_2 slurries were similar (30 to 40 nm),and were also similar to the CeO_2 NPs. The broader range of primary particle sizes for the Al_2O_3 resulted in a larger mean diameter and larger size distribution than the other NPs. Differences between SEM and TEM analysis was low (Table 3), except for the Al_2O_3 NPs, which may have been associated with the modest number of primary particles counted given the large observed distribution in diameters.

The particle size distribution of slurries diluted approximately 10:1 with DI water was also analyzed by DLS in six separate laboratories, resulting in the following mean diameters: 46±10 nm for *c*-SiO_2, 137±10 nm for CeO_2, 141±28 nm for Al_2O_3, and 158±16 nm for *f*-SiO_2. Statistically, there is little difference between the three larger NPs, but in all cases the order of mean sizes was consistent with *c*-SiO_2 having the smallest diameter and Al_2O_3, CeO_2, and *f*-SiO_2 the largest and relatively similar diameter. Differences in absolute diameters may be attributed to six different operators and three instrument models that used different laser wavelengths (659, 488, 633 nm) and different scattering angles (90°, 90°, 173°). The hydrodynamic diameter of the CMP NPs was larger compared to the size determined for the primary particles by electron microscopy (Table 3). *c*-SiO_2 was an exception, and the particle size determined with these two

techniques was relatively similar. In contrast, the DLS sizing of the *f*-SiO_2 resulted in an average size nearly 2-3 fold higher than determined for the primary NPs, reflective of the aggregated nature of the primary NPs into a dendritic morphology, and the hydrodynamic size of the CeO_2 NPs was approximately two-fold higher compared to the primary particle size determined by electron microscopy (Table 3, Fig. 6).

The NTA trends in NP size from smallest to largerst were consistent with DLS measurements, with exception of CeO_2, which was sized smaller by NTA (79 nm) than by DLS (132 nm). NTA analysis also determines particle number concentrations, which were (#particles/ $x10^{12}$ per mL): 4.7 ± 0.2 for *c*-SiO_2, 13.0 ± 0.3 for *f*-SiO_2, 3.9 ± 0.2 for CeO_2, and 22.0 ± 1.1 for Al_2O_3.

An additional sizing method, spICP-MS, was also employed to evaluate the particle size distribution in the CMP slurries (Fig. 7). In this method, the cloud of ions generated from the ablation of a single particle is detected as a pulse above the background by utilizing short dwell times. Calculated mean diameters from spICP-MS analysis were 144 ± 26, 60 ± 28, and 66 ± 23 nm for *f*-SiO_2, CeO_2, and Al_2O_3, respectively. Limitations brought on by molecular interfering ions (e.g., dinitrogen) hindered the sizing of the SiO_2 NPs below 100 nm and biased the diameter toward a larger mean size than actually present in the sample. The average particle sizes determined for *f*-SiO_2 using spICP-MS, DLS, and NTA are very similar (Table 3). The size of *c-SiO₂* was below current spICP-MS detection limits for silica, indicating it has smaller diameter than *f-SiO₂*, which is consistent with DLS, NTA, and SEM/TEM. Advances in micro-second dwell time ICP-MS technology and analysis may be capable of improving size resolution for *c-SiO₂* or other NPs with high background noise or poor detection resolution [45, 46]. Mean diameters for Al_2O_3 and CeO_2 by spICP-MS were similar to each other and between electron microscopy methods and DLS or NTA results. The size distributions of NPs based upon spICP-MS lose some resolution relative to background below ~25 nm for Al_2O_3 and CeO_2, which biases the mean to slightly larger sizes. The size ranges near the peak of the Gaussian distributions (Fig. 7) are in closer agreement with SEM/TEM results.

Few studies compare size measurements across as many techniques on the same number of different, well-dispersed NPs as present in these CMP slurries. Fig. 8 compares mean diameters reported by the manufacturer to those measured by the various techniques reported herein. Within any single evaluation technique, the size trends from smallest to largest are generally

consistent, but significant differences in absolute size vary dramatically. This points to both the bias and assumptions of each technique (e.g., hydrated radius, mineral structure, density). Whereas DLS and NTA detect the hydrodynamic size, spICP-MS and SEM/TEM are not impacted by the hydrated nature of NPs and thus hydrodynamic state partially accounts for observed differences in mean diameters reported in Table 3 and shown in Fig. 8.

3.4. Stability of Nanoparticles in Different Matrices

Surface charge is a critical factor influencing the stability (i.e., aggregation potential) of NP dispersions. Zeta potential measurements of the CMP slurries (Table 3), diluted with ultrapure water to concentrations suitable for zeta potential analysis, resulted in highly positively charged NPs (> +40 mV) for CeO_2 and Al_2O_3 or very negatively charged (< -20 mV) for the two SiO_2 NPs. Zeta potentials this far from zero indicate very stable NP suspensions. The manufacturer claims that the NPs in the CMP slurries would remain stable for at least two years if stored in the dark at room temperature. Fig. 9 shows both the zeta potentials and DLS measurements obtained at the same time. Separate measurements performed six months later showed no discernible differences in zeta potential or DLS.

Fig. 10 shows the electrophoretic mobilities (EPMs) of four CMP NPs as a function of pH. At pH higher than 2, the *c*-SiO_2 and *f*-SiO_2 were negatively charged, and the magnitude of surface charge generally increased with increasing pH. The *f*-SiO_2 was almost neutral at pH 2, which is consistent with the reported pH of zero point of charge (pH_{ZPC}) of 2.0 for SiO_2 [47]. The pH_{ZPC} of *c*-SiO_2 was lower than 2. CeO_2 and Al_2O_3 colloids were both positively charged at pH lower than 7.0, and their surface charges reversed when pH was elevated to 11. By extrapolation, the pH_{ZPC} for CeO_2 and Al_2O_3 colloids were determined to be approximately 8 and 10, respectively, which are consistent with the reported pH_{ZPC} for CeO_2 (8.1) [48] and for Al_2O_3 (8.2–10) [49].

3.5. Surface Reactivity of Silica Nanomaterials

The CADE uses the reduction rate of methylene blue by borohydride, which depends directly on the catalytic activity of nanoparticles in CMP. Results in SI showed a statistical differences at the 95% confidence interval between the catalytic reactivity in a control from the catalytic activity induced by *f*- or *c*-SiO_2 present at 100 ppm. The *f*-SiO_2 nanoparticles were also more

catalytically active than the *c-SiO₂* nanoparticles from CMP slurries. At fixed CMP mass concentration, the surface charge of nanoparticles may have an influence on the catalytic reactivity of CMPs. We believe negatively charged particles, *c*-SiO_2 and *f*-SiO_2, with a surface charge of -21 and -50 mV, may electrostatically repel BH_4 molecules to the surface of the particle, which then inhibit the reduction of MB, resulting in high β values. According to Azad et al. when BH_4 absorbs to the surface of nanoparticles, it creates a negatively charged layer that attracts cationic organic dyes, such as CADE [50]. This electrostatic attraction or repulsion between particle surfaces and the reducing agents increase or decrease the reduction rate of MB.

3.6. *In Vitro* Toxicity

The potential toxicity of model CMP slurries to bacteria *A. fischeri* was assessed using the Microtox® assay. Microtox® assay is a highly sensitive test that is widely used to monitor the toxicity of effluents and evaluate the toxic effects of chemical compounds [51]. The results of the test have been shown to correlate well with toxicity values for fish, crustaceans, and algae for a wide range of organic and inorganic chemicals. The results in Table 4 indicate that the CMP NPs were not or only mildly inhibitory to the metabolic activity of *A. fischeri* at high concentrations ranging from 0.7 to 1.3 mg/mL, depending on the assay. No effect was observed when cells were exposed to *f*-SiO_2 and CeO_2 NPs. This observation is similar to the CADE analysis shows that *f*-SiO_2 posses higher catalytic reactivity than *c*-SiO_2, where surface redox reactivity in nanoparticles is a key emerging property related to potential cellular toxicity. Exposure to a concentration of 1.3 mg/mL of the *c*-SiO_2 and Al_2O_3 suspensions resulted in 37.6 and 28.4% inhibition, respectively.

For the eukaryote toxicity tests with A549 cells, the IC-50 values for proliferation and plasma membrane integrity were in the range 1 to 4 mg/mL for both *c*-SiO_2 and *f*-SiO_2. The viability tests using MTT resulted in IC-50 values for both forms of SiO_2 in the range of 1 to 2 mg/mL. The CeO_2 and Al_2O_3 had negligible effect in any of the A549 cell assays at the highest tested slurry concentrations. In both prokaryotic and eukaryotic cell assays, the CMP NPs were unstable and aggregated when in biological medium. This was especially pronounced for CeO_2 and Al_2O_3.

With the prokaryote *A. fischeri*, none of the CMP metal oxides NPs resulted in as much as a 50% decrease in bioluminescence in the Microtox® assay after a 30 min exposure. Thus, CMP

NPs do not appear to be very toxic to *A. fischeri*. However, there was a statistically significant reduction in bioluminescence from bacteria exposed to *c*-SiO_2 and Al_2O_3 at 1.3 mg/mL for 30 min (37.6 and 28.4% inhibition, respectively). It is therefore likely that there could be more significant adverse effects at higher doses and longer exposure times. Literature results confirm the low toxicity of silica, ceria, and alumina NPs towards *A. fischeri*. No appreciable effects were observed in Microtox® assays supplemented with nominal concentrations of CeO_2 and Al_2O_3 up to 0.1 mg/mL [52, 53]. Similarly, amorphous SiO_2 NPs of different diameters (50 and 100 nm) were not toxic to *A. fischeri* at a concentration as high as 1 mg/mL.

There are many studies in the literature on the toxicity of SiO_2 NPs towards various cultured mammalian cells with a wide range of toxicity values reported. Factors that influence silica NP toxicity include cell type, differences in the physical and surface properties of the NPs, and the type of toxicity assay [54-57]. The IC-50 values reported here for the various assays with A549 cells (in the range of 1 to 4 mg/mL for a 24 hour exposure) are consistent with data in the literature. For example, Lin et al. (2006) observed at most a 17% reduction in viability after exposing A549 cells to 15 nm SiO_2 NPs for 24 hours, and at 72 h exposure the viability was reduced by about half [58]. Yu et al. (2011) reported no effect of *c*-SiO_2 colloidal silica on A549 cells in a 24 h exposure up to the highest concentration tested of 0.5 mg/mL [55]. Yu et al. (2011) also reported that a murine macrophage cell line (RAW 264.7) responded to *c*-SiO_2 with an IC-50 of ~200 μg/mL, emphasizing that different cell types may respond differently to SiO_2. Using the MTT assay and an impedance-based assay, Otero-Gonzalez et al. (2012) found IC-50 values in the range of 0.17-0.23 mg/mL with human bronchial epithelial cells (16HBE14o-) exposed to amorphous SiO_2 for 48 h [59]. Zhang et al. (2012) reported that *f*-SiO_2 prepared by a high temperature process was significantly more toxic than *c*-SiO_2 prepared by a low temperature process [56]. They attributed the result to different surface chemistries generated by the different synthesis methods. Nevertheless, we observed little difference in the toxicity of colloidal and fumed SiO_2 in a variety of assays with A549 cells.

The biological effects of CeO_2 have been enigmatic because of reports that it is both an oxidant capable of generating reactive oxygen species (ROS) and an anti-oxidant capable of protecting cells from oxidants by consuming ROS [60]. The different oxidation properties are attributed to the presence of both Ce(III) and Ce(IV) in NPs. Interpretation of the literature has been confusing because the same type of NP could seemingly be oxidizing or anti-oxidizing,

toxic or non-toxic. Recent work from the Baer group has brought insight to the problem [61]. CeO_2 is usually made by one of three methods: high temperature heating (> 300°C), heated in a solvent (< 100°C), or prepared at room temperature. Karakoti et al. (2012) grouped biological responses to CeO_2 in the literature according to synthesis method and noticed that most (but not all) of the CeO_2 made by the high temperature or high temperature in solvent methods were either pro-oxidative or had both oxidative and anti-oxidative properties as reported in the various assays used in papers [61]. CeO_2 made at room temperature was, with one exception, anti-oxidative. This analysis is another example demonstrating that the method of nanoparticle synthesis can have a large influence on its properties and biological effects. However, the CMP CeO_2 NPs we examined had no measureable toxicity in our A549 assays up to the highest concentrations tested.

As with many nanomaterials, there is a diversity of literature and opinions on whether Al_2O_3 NPs are toxic. For example, nano-Al_2O_3 at 100 to 1000 mg/L was toxic to cultured human brain microvascular endothelial cells and also reduced tight junctions in brain endothelial cells in cerebral vasculature after infusion into rats [62]. Al_2O_3 NPs were at least mildly toxic to osteoblast-like UMR 106 cells using assays of mitochondrial and lysosome function [63], and they were cytotoxic and genotoxic with CHO-K1 cells [64]. Otero-Gonzalez et al. (2012) observed that exposing human bronchial epithelial cells (16HBE14o-) to 1 mg/mL of nano-Al_2O_3 (< 50 nm) for 48 h resulted in 50% inhibition in the MTT assay[59]. In the same study, the IC-50 value determined for nano-Al_2O_3 using an impedance-based real-time cell analyzer was 0.3 mg/mL. In recent work, Al_2O_3 NPs were reported toxic to plant cells in culture and toxic to fresh water algae [65, 66]. In contrast, Al_2O_3 NPs had no measurable toxicity with mouse L929 cells and normal human fibroblasts [67]. Moreover, even at high concentrations, nano-Al_2O_3 did not affect the phagocytic activity of rat alveolar macrophages [68]. Our results with Al_2O_3 CMP slurry failed to find any toxic response with A549 cells in three different types of assays.

Toxicity data developed herein for *f*- SiO_2 and *c*-SiO_2, Al_2O_3, and CeO_2 were integrated with human and other organisms. These data are summarized along with corresponding IC-50 and the half maximal effective concentration (EC-50) data reported in the literature in Figures 11 and 12. The IC/EC-50 concentrations for silica are higher than for alumina, which in turn is higher than for ceria. This is good because it is in reverse order of their prevalence and use in most semiconductor fabrication facilities (fabs). Silica, which is used in most abundance, generally

546 has the highest IC/EC-50 values and is therefore least toxic. It is evident that for a given material
547 type, there is considerable variation among the IC/EC-50 data, depending upon the particular test
548 type, cell line or test organism, test duration, and test endpoint.
549
550 **4. Impact of Findings on Semiconductor Industry**
551 Another key aspect of this work has been a collaborative effort between universities and the
552 semiconductor industry to determine the conditions and concentration ranges necessary for the
553 ENP analytical methods. Using a materials balance from one fab and drawing from reported
554 concentration data in the literature (see Supplemental Information), SiO_2 concentrations in the
555 effluent wastewater that comes directly from CMP operations, but prior to treatment, might
556 typically be on the order of 1,000 mg/L, alumina concentrations on the order of 10 to 100 mg/L,
557 and cerium concentrations on the order of 1 mg/L or less. Cerium is less prevalently used than
558 either silica or alumina in CMP operations, and none of the referenced literature reports listed
559 cerium concentration in wastewater. According to materials usage records at one fab, silica,
560 alumina, and ceria may be used in proportions of roughly 90:9:1. However, slurry formulations
561 are both proprietary and dynamic.
562 There are also significant differences between fabs in the manner that CMP wastewater is
563 routed through the fab and treated. Some, like the fab described in Supplemental Information,
564 employ a physical-chemical wastewater treatment system for the composite CMP water,
565 followed by dilution and equalization with other on-site wastewater flows before treatment by an
566 on-site biological wastewater system. For this particular fab, the waste streams that represent
567 potential gateways for releasing Al_2O_3, CeO_2, and SiO_2 ENPs to the environment are the solids
568 concentrate produced by the CMP wastewater treatment process and/or discharges from
569 municipal wastewater treatment plants that receive sewer discharges from the fab. In this fab, the
570 on-site industrial CMP wastewater treatment process produces a filter cake with a 52% water
571 content and measured SiO_2 and Al_2O_3 concentrations of 77 and 8 wt%, respectively. Although
572 this particular filter cake was recycled for the production of cement, it demonstrates the
573 importance of evaluating the fate and long term stability of the solids concentrate waste streams
574 from on-site CMP wastewater treatment processes as the ENP composition of waste sludges may
575 range from less than 1 wt % to greater than 75 wt %. The treated effluent from municipal
576 biological wastewater treatments is typically discharged to surface waters, and the waste sewage

sludges or biosolds disposed as land soil amendments (~60%), landfills (~20%), or incinerated with ash being landfilled (~20%) [69]. SEM analysis of ENPs at the influent and effluent of on-site chemical wastewater treatment processes at a fab (see SI) indicate the presence of SiO_2 ENPs. While both locations have ENPs approximately 70 nm in size, the effluent SiO_2 NPs appear to have slightly different surface morphologies. Overall, the results and analytical methods herein with the four CMP slurries can be applied to effluent streams in fabs to determine ENP behavior and fate. Ideally, speciated and size fractionated ENP concentration data are available for the influent, effluent, and waste biosolids, such that a materials balance account can be made across wastewater treatment facilities.

Analytical method development is relevant not only for assessing the fate of ENPs, but also for determining their impact on biological processes (industrial on-site or off-site municipal facilities). For instance, Zheng et al. (2012) reported 35 % inhibition of N removal efficiency at 50 mg/L of 80 nm SiO_2 [70]. Others observed a 37% inhibition of O_2 uptake rate for 50 mg/L of 50 nm SiO_2 [71]. Details for a particular fab with on-site chemical and biological treatment are provided in SI. The mass balance indicates 2 mg/L of SiO_2 influent to the on-site treatment facility and 0.2 mg/L in the effluent from the biological wastewater treatment step. Thus, the biological treatment is important in reducing ENP levels. If a fab doesn't pre-treat waste streams in the fab or have extensive dilution with other on-site wastewater flows, its potential ENP influent concentrations to the biological treatment process could be several tens of mg/l or greater, which may inhibit the performance of the biological wastewater treatment process.

4. Conclusions

A principal objective of this work was to develop a common set of ENP samples that could be shared between different laboratories and used to develop validated analytical methods for characterizing CMP slurries and their associated waste streams. The ENPs in the "model slurries" are representative of those used in commercial CMP slurries, but they lack the additives that are commonly employed in commercial slurries and thus are intended as only a first step in analytical method development. Moreover, the four test slurries are models of the raw unused slurries prior to contact with wafers in CMP operations, and so likewise these model slurries serve as only a first step towards our ultimate goal of using validated methods to characterize the behavior and fate of alumina, ceria, and silica ENPs in real fab wastewaters and effluent

discharges. Towards these goals we have developed metal oxide digestion methods that are appropriate for determining *f*-SiO_2 and *c*-SiO_2, Al_2O_3, and CeO_2 concentrations. We have demonstrated two alternative methods, a centrifuge and an ultrafiltration method, for distinguishing between dissolved and ENP concentrations. We have demonstrated the applicability of four different particle size distribution methods and highlighted their relative differences.

Cytotoxicity using prokaryotic and eukaryotic toxicity assays showed a low inhibitory potential of the four ENPs in the CMP slurries. The concentrations of ENPs in all four slurries causing 50% inhibition (IC-50) were greater than 1 mg/mL based upon *in vitro* assays using bioluminescence of the bacterium *Aliivibrio fischeri* and proliferation and viability or integrity of human cells (adenocarcinomic human alveolar basal epithelial cell line A549). Based on these IC-50 values, none of these model slurry dispersions showed acute toxicity in assays performed. In contrast with some previous reports, *f*-SiO_2 was not significantly more toxic than *c*-SiO_2 in the CMP slurries, despite having different sizes and morphologies but similar characterization by FTIR and XRD. Additional characterization techniques that probe surface reactivity or number and proximity of surface hydroxyl groups are needed to improve our understanding of discrepancies in the literature. Otherwise, the levels of toxicity of the ENPs towards human cells or model aquatic organisms were similar to literature reports and suggest monitoring at mg/L levels would be adequate to meet IC-50 levels. IC-50 values (> 1000 mg/L) are much higher than ENP concentrations expected in semiconductor effluents,. It should be noted that the general practice in the CMP industry is to dilute the slurry waste stream so actual abrasive concentrations are typically orders of magnitude smaller than 1 mg/mL, which is lower than IC-50 levels.

Among the most interesting observations was the ability of the CMP slurry manufacturer to produce 1 to > 5 wt% ENPs that have remained dispersed in solution for many months (i.e., stable; no aggregation). The special-order slurries did not contain organic surfactants, and we demonstrated through comprehensive analysis of the solution that there were no added stabilizers other than pH adjustment. The slurry manufacturers were able to disperse the ENPs using mechanical, sound, or other non-chemical means and then maintain a very highly negative (less than -20 mV for *c*- and *f*-SiO_2) or very highly positive (greater than +40 mV for Al_2O_3 and CeO_2) zeta potential through pH adjustment.

The size, morphology, and composition of the ENPs in the CMP slurries differed. Size measurements by TEM, SEM, and spICP-MS agreed well and were smaller than measurements by DLS and NTA, which accounted for the hydrodynamic influence of the nanoparticles. There was excellent agreement among multiple laboratories performing DLS measurements on the well-dispersed ENPs. *f*-SiO_2 ENPs contained small primary particles agglomerated together into dendritic structures whereas the *c*-SiO_2 ENPs were present as small and usually singular (non-agglomerated) particles, indicating that the synthesis method impacts the morphology more than structural properties measured by FTIR, XRD, or XPS. CeO_2 ENPs were cubic shaped and generally not-agglomerated whereas Al_2O_3 nanoparticles contained a wide range of primary particle sizes and were agglomerated together. Elemental analysis of the ENPs (Fig. 2) revealed the presence of trace constituents that, while representing low weight percentages of the nanoparticles, might influence their reactivity and or ability to be traced in the environment. Such elemental data has not been reported for other nanoparticles, and the presence of some metals may be related to the purity of silica, ceria, or alumina used in bulk by the CMP slurry manufacturer, compared against high grade purity levels typically used in laboratory studies that synthesize nanoparticles for specific research applications. Unrelated observations, yet similar conclusions, have been reported when yttrium and other trace metals were reported in carbon nanotubes [72]. Additional research is needed to understand the implications of differences in stock reagent purity on nanoparticle properties as production of ENPs scales up.

Acknowledgements

This work was supported by the Semiconductor Research Corporation (SRC) Engineering Research Center for Environmentally Benign Semiconductor Manufacturing and the University of Arizona Water Sustainability Program. Gratitude is extended to Cabot Inc. for preparing the CMP slurries used in this study, which are now available through Farhang Shadman (Univ of Arizona) for other research groups to apply in EHS or other nano-related studies. This work was partially funded by the USEPA (grant number RD83558001).

Appendix. Supplementary Data

669

670 Supplementary information includes some analytical methods and in-depth discussion of ENP
671 fate during on-site industrial wastewater treatment.

672

673

674 References

675 1. Keller, A. A.; Lazareva, A., Predicted releases of engineered nanomaterials:From global
676 to regional to local. *Environ. Sci. Tech. Letters* **2014,** *1*, (1), 65-70.
677 2. Kroll, A.; Dierker, C.; Rommel, C.; Hahn, D.; Wohlleben, W.; Schulze-Isfort, C.;
678 Goebbert, C.; Voetz, M.; Hardinghaus, F.; Schnekenburger, J., Cytotoxicity screening of 23
679 engineered nanomaterials using a test matrix of ten cell lines and three different assays. *Particle*
680 *and Fibre Toxicology* **2011,** *8*.
681 3. Maynard, A. D.; Warheit, D. B.; Philbert, M. A., The New Toxicology of Sophisticated
682 Materials: Nanotoxicology and Beyond. *Toxicological Sciences* **2011,** *120*, S109-S129.
683 4. Nel, A. E.; Nasser, E.; Godwin, H.; Avery, D.; Bahadori, T.; Bergeson, L.; Beryt, E.;
684 Bonner, J. C.; Boverhof, D.; Carter, J.; Castranova, V.; DeShazo, J. R.; Hussain, S. M.; Kane, A.
685 B.; Klaessig, F.; Kuempel, E.; Lafranconi, M.; Landsiedel, R.; Malloy, T.; Miller, M. B.; Morris,
686 J.; Moss, K.; Oberdorster, G.; Pinkerton, K.; Pleus, R. C.; Shatkin, J. A.; Thomas, R.; Tolaymat,
687 T.; Wang, A.; Wong, J., A Multi-Stakeholder Perspective on the Use of Alternative Test
688 Strategies for Nanomaterial Safety Assessment. *Acs Nano* **2013,** *7*, (8), 6422-6433.
689 5. Oberdorster, G., Safety assessment for nanotechnology and nanomedicine: concepts of
690 nanotoxicology. *Journal of Internal Medicine* **2010,** *267*, (1), 89-105.
691 6. Handy, R. D.; Cornelis, G.; Fernandes, T.; Tsyusko, O.; Decho, A.; Sabo-Attwood, T.;
692 Metcalfe, C.; Steevens, J. A.; Klaine, S. J.; Koelmans, A. A.; Horne, N., Ecotoxicity test methods
693 for engineered nanomaterials: Practical experiences and recommendations from the bench.
694 *Environ. Toxicol. Chem.* **2012,** *31*, (1), 15-31.
695 7. von der Kammer, F.; Ferguson, P. L.; Holden, P. A.; Masion, A.; Rogers, K. R.; Klaine,
696 S. J.; Koelmans, A. A.; Horne, N.; Unrine, J. M., Analysis of engineered nanomaterials in
697 complex matrices (environment and biota): General considerations and conceptual case studies.
698 *Environ. Toxicol. Chem.* **2012,** *31*, (1), 32-49.
699 8. Jarvie, H. P.; Al-Obaidi, H.; King, S. M.; Bowes, M. J.; Lawrence, M. J.; Drake, A. F.;
700 Green, M. A.; Dobson, P. J., Fate of Silica Nanoparticles in Simulated Primary Wastewater
701 Treatment. *Environmental Science & Technology* **2009,** *43*, (22), 8622-8628.
702 9. Limbach, L. K.; Bereiter, R.; Mueller, E.; Krebs, R.; Gaelli, R.; Stark, W. J., Removal of
703 oxide nanoparticles in a model wastewater treatment plant: Influence of agglomeration and
704 surfactants on clearing efficiency. *Environmental Science & Technology* **2008,** *42*, (15), 5828-
705 5833.
706 10. Gomez-Rivera, F.; Field, J. A.; Brown, D.; Sierra-Alvarez, R., Fate of cerium dioxide
707 (CeO2) nanoparticles in municipal wastewater during activated sludge treatment. *Bioresource*
708 *Technology* **2012,** *108*, 300-304.
709 11. Kiser, M. A.; Westerhoff, P.; Benn, T.; Wang, Y.; Perez-Rivera, J.; Hristovski, K.,
710 Titanium Nanomaterial Removal and Release from Wastewater Treatment Plants. *Environ. Sci.*
711 *Tech.* **2009**.

12. Kiser, M. A.; Westerhoff, P. K.; Ryu, H.; Benn, T., Occurrence and fate of engineered nanomaterials in wastewater treatment plants. *Abstracts of Papers of the American Chemical Society* **2010,** *240*.
13. Barton, L. E.; Auffan, M.; Bertrand, M.; Barakat, M.; Santaella, C.; Mason, A.; Borschneck, D.; Olivi, L.; Roche, N.; Wiesner, M. R.; Bottero, J.-Y., Transformation of Pristine and Citrate-Functionalized CeO2 Nanoparticles in a Laboratory-Scale Activated Sludge Reactor. *Environmental Science & Technology* **2014,** *48*, (13), 7289-7296.
14. Rottman, J.; Shadman, F.; Sierra-Alvarez, R., Interactions of inorganic oxide nanoparticles with sewage biosolids. *Water Science and Technology* **2012,** *66*, (9), 1821-1827.
15. Wiesner, M. R.; Lowry, G. V.; Casman, E.; Bertsch, P. M.; Matson, C. W.; Di Giulio, R. T.; Liu, J.; Hochella, M. F., Jr., Meditations on the Ubiquity and Mutability of Nano-Sized Materials in the Environment. *Acs Nano* **2011,** *5*, (11), 8466-8470.
16. Conrad, C. F.; Icopini, G. A.; Yasuhara, H.; Bandstra, J. Z.; Brantley, S. L.; Heaney, P. J., Modeling the kinetics of silica nanocolloid formation and precipitation in geologically relevant aqueous solutions. *Geochim. Cosmochim. Acta* **2007,** *71*, (3), 531-542.
17. Krishnan, M.; Nalaskowski, J. W.; Cook, L. M., Chemical Mechanical Planarization: Slurry Chemistry, Materials, and Mechanisms. *Chem. Rev.* **2010,** *110*, (1), 178-204.
18. Zantye, P. B.; Kumar, A.; Sikder, A. K., Chemical mechanical planarization for microelectronics applications. *Materials Science & Engineering R-Reports* **2004,** *45*, (3-6), 89-220.
19. Singh, R. K.; Bajaj, R., Advances in chemical-mechanical planarization. *MRS bulletin* **2002,** *27*, (10), 743-751.
20. Feng, X.; Sayle, D. C.; Wang, Z. L.; Paras, M. S.; Santora, B.; Sutorik, A. C.; Sayle, T. X.; Yang, Y.; Ding, Y.; Wang, X., Converting ceria polyhedral nanoparticles into single-crystal nanospheres. *Science* **2006,** *312*, (5779), 1504-1508.
21. Brown, K. H.; Grose, D. A.; Lange, R. C.; Ning, T. H.; Totta, P. A., Advancing the state of the art in high-performance logic and array technology. *IBM journal of research and development* **1992,** *36*, (5), 821-828.
22. Krishnan, M.; Nalaskowski, J. W.; Cook, L. M., Chemical mechanical planarization: slurry chemistry, materials, and mechanisms. *Chemical reviews* **2009,** *110*, (1), 178-204.
23. Zantye, P. B.; Kumar, A.; Sikder, A., Chemical mechanical planarization for microelectronics applications. *Materials Science and Engineering: R: Reports* **2004,** *45*, (3), 89-220.
24. Liu, Y.; Zhang, K.; Wang, F.; Di, W., Investigation on the final polishing slurry and technique of silicon substrate in ULSI. *Microelectronic Engineering* **2003,** *66*, (1), 438-444.
25. Willardson, R. K.; Weber, E. R.; Li, S. M. H.; Miller, R. M., *Chemical mechanical polishing in silicon processing*. Academic press: 1999; Vol. 63.
26. Iler, R. K., The chemistry of silica: solubility, polymerization, colloid and surface properties, and biochemistry. **1979**.
27. Stöber, W.; Fink, A.; Bohn, E., Controlled growth of monodisperse silica spheres in the micron size range. *Journal of colloid and interface science* **1968,** *26*, (1), 62-69.
28. Wang, Z. L.; Feng, X., Polyhedral shapes of CeO2 nanoparticles. *The Journal of Physical Chemistry B* **2003,** *107*, (49), 13563-13566.
29. Schroeder, D. J.; Moeggenborg, K. J.; Chou, H.; Chamberlain, J. P.; Hawkins, J. D.; Carter, P., CMP method utilizing amphiphilic nonionic surfactants. In Google Patents: 2005.

30. Coetsier, C. M.; Testa, F.; Carretier, E.; Ennahali, M.; Laborie, B.; Mouton-arnaud, C.; Fluchere, O.; Moulin, P., Static dissolution rate of tungsten film versus chemical adjustments of a reused slurry for chemical mechanical polishing. *Applied Surface Science* **2011,** *257*, (14), 6163-6170.
31. Testa, F.; Coetsier, C.; Carretier, E.; Ennahali, M.; Laborie, B.; Serafino, C.; Bulgarelli, F.; Moulin, P., Retreatment of silicon slurry by membrane processes. *J Hazardous Materials* **2011,** *192*, (2), 440-450.
32. Song, X. L.; Jiang, N.; Li, Y. K.; Xu, D. Y.; Qiu, G. Z., Synthesis of CeO2-coated SiO2 nanoparticle and dispersion stability of its suspension. *Materials Chemistry and Physics* **2008,** *110*, (1), 128-135.
33. Elimelech, M.; Gregory, J.; Jia, X.; Williams, R. A., Particle Deposition and Aggregation - Measurement, Modelling and Simulation. In Butterworth-Heinemann: Oxford: England, 1995.
34. Degueldre, C.; Favarger, P. Y.; Wold, S., Gold colloid analysis by inductively coupled plasma-mass spectrometry in a single particle mode. *Anal. Chim. Acta* **2006,** *555*, (2), 263-268.
35. Pace, H. E.; Rogers, N. J.; Jarolimek, C.; Coleman, V. A.; Higgins, C. P.; Ranville, J. F., Determining Transport Efficiency for the Purpose of Counting and Sizing Nanoparticles via Single Particle Inductively Coupled Plasma Mass Spectrometry. *Analytical Chemistry* **2011,** *83*, (24), 9361-9369.
36. Pace, H. E. R., N. J.; Jarolimek, C.; Coleman, V. A.; Gray, E. P.; Higgins, C. P.; Ranville, J. F., Single particle inductively coupled plasma-mass spectrometry: a performance evaluation and method comparison in the determination of nanoparticle size. *Environ. Sci. Technol.* **2012,** *46*.
37. Corredor, C.; Borysiak, M.; Wolfer, J.; Westerhoff, P.; Posner, J., Colorimetric Detection of Catalytic Reactivity of Nanoparticles in Complex Matrices. *Environ. Sci. Technol.* **2015**.
38. Gondikas, A. P.; von der Kammer, F.; Reed, R. B.; Wagner, S.; Ranville, J. F.; Hofmann, T., Release of TiO2 Nanoparticles from Sunscreens into Surface Waters: A One-Year Survey at the Old Danube Recreational Lake. *Environmental Science & Technology* **2014,** *48*, (10), 5415-5422.
39. Gu, H.; Soucek, M. D., Preparation and characterization of monodisperse cerium oxide nanoparticles in hydrocarbon solvents. *Chemistry of Materials* **2007,** *19*, (5), 1103-1110.
40. Parida, K. M.; Pradhan, A. C.; Das, J.; Sahu, N., Synthesis and characterization of nano-sized porous gamma-alumina by control precipitation method. *Materials Chemistry and Physics* **2009,** *113*, (1), 244-248.
41. Hsu, P.-Y.; Lin, J.-J.; Lai, B.-W.; Wu, Y.-L.; Yang, C.-F.; Lin, S.-S., FTIR Characterizations of the Gamma-Ray-Irradiated Silica Nanoparticles/ γ -APTES Nanocomposite with UV Annealing. In *Intelligent Technologies and Engineering Systems*, Juang, J.; Huang, Y.-C., Eds. Springer New York: 2013; Vol. 234, pp 893-899.
42. Mackay, R.; Zhang, H.; Wu, Q.; Li, Y. Z., NMR investigation of concentrated alumina and silica slurries. *Colloid Surf. A-Physicochem. Eng. Asp.* **2004,** *250*, (1-3), 343-348.
43. Kuan, W. H.; Hu, C. Y., Chemical evidences for the optimal coagulant dosage and pH adjustment of silica removal from chemical mechanical polishing (CMP) wastewater. *Colloid Surf. A-Physicochem. Eng. Asp.* **2009,** *342*, (1-3), 1-7.
44. Matijevic, E.; Babu, S. V., Colloid aspects of chemical-mechanical planarization. *Journal of Colloid and Interface Science* **2008,** *320*, (1), 219-237.

45. Montano, M. D.; Badiei, H. R.; Bazargan, S.; Ranville, J. F., Improvements in the detection and characterization of engineered nanoparticles using spICP-MS with microsecond dwell times. *Environ.-Sci. Nano* **2014,** *1*, (4), 338-346.
46. Bi, X. Y.; Lee, S.; Ranville, J. F.; Sattigeri, P.; Spanias, A.; Herckes, P.; Westerhoff, P., Quantitative resolution of nanoparticle sizes using single particle inductively coupled plasma mass spectrometry with the K-means clustering algorithm. *J. Anal. At. Spectrom.* **2014,** *29*, (9), 1630-1639.
47. Stumm, W., *Chemistry of the Solid-Water Interface*. Wiley: New York, 1992; p 269-286.
48. Defaria, L. A.; Trasatti, S., THE POINT OF ZERO CHARGE OF CEO2. *J Colloid Interface Sci* **1994,** *167*, (2), 352-357.
49. Kosmulski, M., The pH-dependent surface charging and the points of zero charge. *J Colloid Interface Sci* **2002,** *253*, (1), 77-87.
50. Azad, U. P.; Ganesan, V.; Pal, M., Catalytic reduction of organic dyes at gold nanoparticles impregnated silica materials: influence of functional groups and surfactants. *Journal of Nanoparticle Research* **2011,** *13*, (9), 3951-3959.
51. Johnson, B., Microtox acute toxicity test. In *Freshwater Toxicity Investigations, Part 2*, Blaise, C.; Ferard, J. F., Eds. Springer: Dordrecht, The Netherlands, 2005; pp 69-105.
52. Doshi, R.; Braida, W.; Christodoulatos, C.; Wazne, M.; O'Connor, G., Nano-aluminum: Transport through sand columns and environmental effects on plants and soil communities. *Environ. Res.* **2008,** *106*, (3), 296-303.
53. Velzeboer, I.; Hendriks, A. J.; Ragas, A. M. J.; Van de Meent, D., Aquatic ecotoxicity tests of some nanomaterials. *Environ. Toxicol. Chem.* **2008,** *27*, (9), 1942-1947.
54. Schrurs, F.; Lison, D., Focusing the research effort. *Nature Nanotechnology* **2012,** *7*, (9), 546-548.
55. Yu, T.; Malugin, A.; Ghandehari, H., Impact of Silica Nanoparticle Design on Cellular Toxicity and Hemolytic Activity. *Acs Nano* **2011,** *5*, (7), 5717-5728.
56. Zhang, H.; Dunphy, D. R.; Jiang, X.; Meng, H.; Sun, B.; Tarn, D.; Xue, M.; Wang, X.; Lin, S.; Ji, Z.; Li, R.; Garcia, F. L.; Yang, J.; Kirk, M. L.; Xia, T.; Zink, J. I.; Nel, A.; Brinker, C. J., Processing Pathway Dependence of Amorphous Silica Nanoparticle Toxicity: Colloidal vs Pyrolytic. *Journal of the American Chemical Society* **2012,** *134*, (38), 15790-15804.
57. Schrand, A. M.; Rahman, M. F.; Hussain, S. M.; Schlager, J. J.; Smith, D. A.; Ali, S. F., Metal-based nanoparticles and their toxicity assessment. *Wiley Interdisciplinary Reviews-Nanomedicine and Nanobiotechnology* **2010,** *2*, (5), 544-568.
58. Lin, W.; Huang, Y.-w.; Zhou, X.-D.; Ma, Y., In vitro toxicity of silica nanoparticles in human lung cancer cells. *Toxicology and Applied Pharmacology* **2006,** *217*, (3), 252-259.
59. Otero-Gonzalez, L.; Sierra-Alvarez, R.; Boitano, S.; Field, J. A., Application and Validation of an Impedance-Based Real Time Cell Analyzer to Measure the Toxicity of Nanoparticles Impacting Human Bronchial Epithelial Cells. *Environmental Science & Technology* **2012,** *46*, (18), 10271-10278.
60. Karakoti, A.; Singh, S.; Dowding, J. M.; Seal, S.; Self, W. T., Redox-active radical scavenging nanomaterials. *Chem. Soc. Rev.* **2010,** *39*, (11), 4422-4432.
61. Karakoti, A. S.; Munusamy, P.; Hostetler, K.; Kodali, V.; Kuchibhatla, S.; Orr, G.; Pounds, J. G.; Teeguarden, J. G.; Thrall, B. D.; Baer, D. R., Preparation and characterization challenges to understanding environmental and biological impacts of ceria nanoparticles. *Surface and Interface Analysis* **2012,** *44*, (8), 882-889.

62. Chen, L.; Yokel, R. A.; Hennig, B.; Toborek, M., Manufactured Aluminum Oxide Nanoparticles Decrease Expression of Tight Junction Proteins in Brain Vasculature. *Journal of Neuroimmune Pharmacology* **2008,** *3*, (4), 286-295.
63. Di Virgilio, A. L.; Reigosa, M.; Fernandez Lorenzo de Mele, M., Response of UMR 106 cells exposed to titanium oxide and aluminum oxide nanoparticles. *Journal of Biomedical Materials Research Part A* **2010,** *92A*, (1), 80-86.
64. Di Virgilio, A. L.; Reigosa, M.; Arnal, P. M.; Fernandez Lorenzo de Mele, M., Comparative study of the cytotoxic and genotoxic effects of titanium oxide and aluminium oxide nanoparticles in Chinese hamster ovary (CHO-K1) cells. *J Hazardous Materials* **2010,** *177*, (1-3), 711-718.
65. Pakrashi, S.; Dalai, S.; Prathna, T. C.; Trivedi, S.; Myneni, R.; Raichur, A. M.; Chandrasekaran, N.; Mukherjee, A., Cytotoxicity of aluminium oxide nanoparticles towards fresh water algal isolate at low exposure concentrations. *Aquatic Toxicology* **2013,** *132*, 34-45.
66. Poborilova, Z.; Opatrilova, R.; Babula, P., Toxicity of aluminium oxide nanoparticles demonstrated using a BY-2 plant cell suspension culture model. *Environmental and Experimental Botany* **2013,** *91*, 1-11.
67. Radziun, E.; Wilczynska, J. D.; Ksiazek, I.; Nowak, K.; Anuszewska, E. L.; Kunicki, A.; Olszyna, A.; Zabkowski, T., Assessment of the cytotoxicity of aluminium oxide nanoparticles on selected mammalian cells. *Toxicol. Vitro* **2011,** *25*, (8), 1694-1700.
68. Wagner, A. J.; Bleckmann, C. A.; Murdock, R. C.; Schrand, A. M.; Schlager, J. J.; Hussain, S. M., Cellular interaction of different forms of aluminum nanoparticles in rat alveolar macrophages. *Journal of Physical Chemistry B* **2007,** *111*, (25), 7353-7359.
69. Westerhoff, P.; Lee, S.; Yang, Y.; Gordon, G.; Hristovski, K.; Halden, R. U.; Herckes, P., Examination of opportunities for metal prospecting in municipal biosolids by analysis of samples from full scale wastewater treatment plants *Environ. Sci. Technol.* **2015**.
70. Zheng, X.; Su, Y.; Chen, Y., Acute and Chronic Responses of Activated Sludge Viability and Performance to Silica Nanoparticles. *Environmental Science & Technology* **2012,** *46*, (13), 7182-7188.
71. Sibag, M.; Choi, B. G.; Suh, C.; Lee, K. H.; Lee, J. W.; Maeng, S. K.; Cho, J., Inhibition of total oxygen uptake by silica nanoparticles in activated sludge. *J Hazardous Materials* **2015,** *283*, 841-846.
72. Reed, R. B.; Goodwin, D. G.; Marsh, K. L.; Capracotta, S. S.; Higgins, C. P.; Fairbrother, D. H.; Ranville, J. F., Detection of single walled carbon nanotubes by monitoring embedded metals. *Environmental Science-Processes & Impacts* **2013,** *15*, (1), 204-213.
73. Holden, P. A.; Klaessig, F.; Turco, R. F.; Priester, J. H.; Rico, C. M.; Avila-Arias, H.; Mortimer, M.; Pacpaco, K.; Gardea-Torresdey, J. L., Evaluation of Exposure Concentrations Used in Assessing Manufactured Nanomaterial Environmental Hazards: Are They Relevant? *Environmental Science & Technology* **2014,** *48*, (18), 10541-10551.
74. Commission, E., Eur. Commission., Commission Staff Working Paper. Types and uses of nanomaterials, including safety aspects, Accompanying the Communication from the Commission to the European Parliament, the Council and the European Economic and Social Committee on the Second Regulatory Review on Nanomaterials; SWD(2012) 288 final; European Commission: Brussels, 3.10.2012, 2012; p 111. http://ec.europa.eu/nanotechnology/pdf/second_regulatory_review_on_nanomaterials_-_staff_working_paper_accompanying_com (2012)_572.pdf (Aug. 15, 2014). . **2012**.

75. Piccinno, F.; Gottschalk, F.; Seeger, S.; Nowack, B., Industrial production quantities and uses of ten engineered nanomaterials in Europe and the world. *Journal Of Nanoparticle Research* **2012,** *14*, (9).

76. Bondarenko, O.; Ivask, A.; Kaekinen, A.; Aruoja, V.; Blinova, I.; Juganson, K.; Kasemets, K.; Kuennis-Beres, K.; Kurvet, I.; Mortimer, M.; Sihtmaee, M.; Kahru, A., Biological effects of nanoparticles of silver, gold, TiO_2 and nanoporous silica to selected invertebrate species and bacteria: FP7 project NanoValid. *Toxicology Letters* **2013,** *221*, S100-S100.

77. Casado, M. P.; Macken, A.; Byrne, H. J., Ecotoxicological assessment of silica and polystyrene nanoparticles assessed by a multitrophic test battery. *Environment International* **2013,** *51*, 97-105.

78. Clement, L.; Zenerino, A.; Hurel, C.; Amigoni, S.; de Givenchy, E. T.; Guittard, F.; Marmier, N., Toxicity assessment of silica nanoparticles, functionalised silica nanoparticles, and HASE-grafted silica nanoparticles. *Science of the Total Environment* **2013,** *450*, 120-128.

79. De Marzi, L.; Monaco, A.; De Lapuente, J.; Ramos, D.; Borras, M.; Di Gioacchino, M.; Santucci, S.; Poma, A., Cytotoxicity and genotoxicity of ceria nanoparticles on different cell lines in vitro. *International Journal of Molecular Sciences* **2013,** *14* (2), 3065-3077.

80. Ji, J.; Long, Z.; Lin, D., Toxicity of oxide nanoparticles to the green algae Chlorella sp. *Chemical Engineering Journal* **2011,** *170* (2-3), 525-530.

81. Lanone, S.; Rogerieux, F.; Geys, J.; Dupont, A.; Maillot-Marechal, E.; Boczkowski, J.; Lacroix, G.; Hoet, P., Comparative toxicity of 24 manufactured nanoparticles in human alveolar epithelial and macrophage cell lines. *Particle and Fibre Toxicology* **2009,** *6*.

82. Lin, W.; Huang, Y.-w.; Zhou, X.-D.; Ma, Y., Toxicity of cerium oxide nanoparticles in human lung cancer cells. *International Journal of Toxicology* **2006,** *25* (6), 451-457.

83. Park, E.-J.; Choi, J.; Park, Y.-K.; Park, K., Oxidative stress induced by cerium oxide nanoparticles in cultured BEAS-2B cells. *Toxicology* **2008,** *245* (1-2), 90-100.

84. Sun, J.; Wang, S.; Zhao, D.; Hun, F. H.; Weng, L.; Liu, H., Cytotoxicity, permeability, and inflammation of metal oxide nanoparticles in human cardiac microvascular endothelial cells. Cytotoxicity, permeability, and inflammation of metal oxide nanoparticles. *Cell Biology and Toxicology* **2011,** *27* (5), 333-342.

85. Yang, S.; Ye, R.; Han, B.; Wei, C.; Yang, X., Ecotoxicological effect of nano-silicon dioxide particles on *Daphnia magna*. *Integrated Ferroelectrics* **2014,** *154* (1), 64-72.

924 **Table 1.** Estimates of the annual production (metric tons/year) of Al_2O_3, CeO_2, and SiO_2.

NP Material Production	Holden et al. (2014) [73]	Keller et al. (2014) [1]	Eur. Comm (2012) [74]	Piccinno et al. (2012) [75]
Al_2O_3	> 200,000	18,500 - 35,000	200,000	55 - 5,500
CeO_2	< 10,000	7,500 - 10,000	10,000	5.5 - 550
SiO_2	> 2,400,000	82,500 - 95,000	1,500,000	55 - 55,000

925

926

927 **Table 2.** Typical CMP slurry additives

Component	Function	Examples
Abrasive particles	Polish surface	Al_2O_3, CeO_2, amorphous SiO_2
pH adjust	Adjust and buffer pH	HCl, KOH, HNO_3, NH_4OH, H_3PO_4, TMAH, NH_4OH, buffers
Complexing agents	Solubilize dissolved metals	Amino acids (glycine, etc), carboxylic acids (citric acid, etc)
Oxidizers	Promote metal removal via oxidative dissolution	H_2O_2, Ferric nitrate, KIO_4, $KMnO_4$, etc.
Corrosion inhibitors	Selectivity against removal of certain surfaces, corrosion inhibition	Benzotriazole (BTA), 3-amino-triazole
Surface active organics	Maintain metal oxide particles in a dispersed state	Polyacrylic acid, polyethylene glycol polymer, cetyl trimethyl ammonium bromide, polyethylene cetyl ether
High MW polymers	Flocculant and/or coat abrasives to "cushion" their abrasiveness	High MW Polyethylene oxide
Biocides	Prevent biological growth	Hydrogen peroxide and others

928

929

930 **Table 3** – Summary of key characteristics for the model CMP slurry composition.

Name	***c*-SiO_2**	***f*-SiO_2**	**CeO_2**	**Al_2O_3**
Manufacturer Reported				
- Material	Colloidal SiO_2	Fumed SiO_2	CeO_2	Al_2O_3
- Composition	3% SiO_2	5% SiO_2	1% CeO_2	3% Al_2O_3
- Additive	< 1% acetic acid	< 1% KOH	none	<1% nitric acid
- pH	2.5 – 4.5	10	3-4	4.5-5.0
- Particle size (nm)	50-60	120-140	60-100	80-100
Primary metal concentration	27 g Si/L	50 g Si/L	9.6 g Ce/L	29 g Al/L
Dissolved organic carbon (DOC; mg/L)	320.5 ± 0.5	4.84 ± 0.03	1.90 ± 0.03	6.77 ± 0.18
Other additives	801.9 ± 1.3 mg/L acetic acid	--	--	134.7 ± 0.8 mg NO_3^-/L BDL* for nitrite
Diameter by SEM (nm)	37 ± 7	38 ± 14	43 ± 16	85± 21
Diameter by TEM (nm)	36 ± 9	ND[#]	39 ± 19	38 ± 16
Mean diameter by DLS (nm)	46 ± 0.2	148 ± 5.1	132 ± 0.1	129± 1.6
(Polydispersity Index)	(0.08)	(0.11)	(0.16)	(0.11)
Diameter by NTA (nm)	61± 0.9	144 ± 1.8	79 ± 1.3	119 ± 1.1
Single particle ICP-MS (nm)	ND	144 ± 26	60 ± 28	66± 23
Zeta potential at slurry pH (mV)	-21	-50	43	55

931

932 * BDL = Below detection limit. [#] particles tended to coalesce, and primary particle size could not be determined.

933

934 **Table 4**. The effects of slurries on the proliferation, viability, or membrane integrity of model
935 organisms. IC-50 levels were not determined (ND) under several conditions as noted.

Assay	**IC-50 (mg/mL)**			
	c-SiO_2	*f*-SiO_2	CeO_2	Al_2O_3
Bioluminescence of *A. fischeri*	ND[1]	ND[2]	ND[3]	ND[4]
Proliferation of A549 cells	3.8± 1.3	3.6 ± 0.2	ND[5]	ND[6]
Viability of A549 cells	1.2 ± 0.2	1.5 ± 0.2	ND[7]	ND[8]
Integrity of A549 cells	4.6 ± 0.2	3.1 ± 0.2	ND[7]	ND[8]

936
937 Notes: [1] 37.6% inhibition at the highest concentration tested (1.3 mg/mL); [2] No effect at highest
938 concentration tested (1.1 mg/mL); [3] Only 4.3% inhibition at the highest concentration tested (0.7
939 mg/mL); [4] Only 28.4% inhibition at the highest concentration tested (1.3 mg/mL); [5] Less than
940 10% inhibition at highest concentration tested (2 mg/mL); [6] 0% inhibition at highest
941 concentration tested (6 mg/mL); [7] No effect at highest concentration tested (0.52 mg/mL); [8] No
942 effect at highest concentration tested (2.0 mg/mL)
943

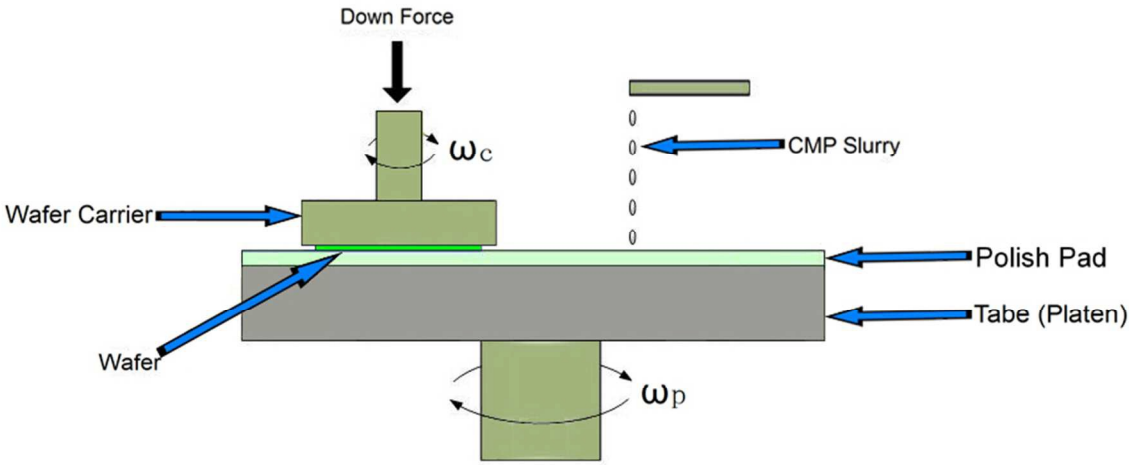

944

945 **Fig. 1.** The CMP operation scheme.

946

947

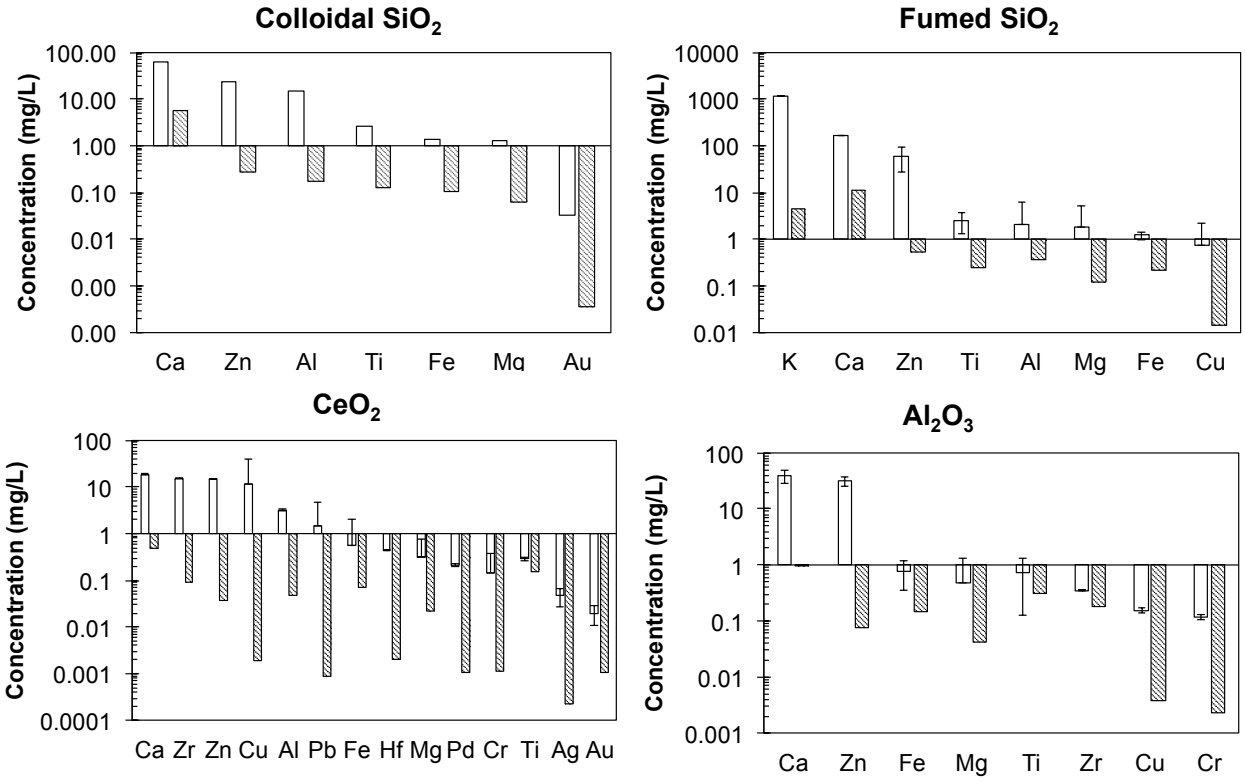

Fig. 2. Concentrations of elements other than the primary metal (Si, Ce or Al) in the four CMP slurries. Open bars represent the element concentration analyzed after a full sample digestion by ICP-MS; shaded bars represent the detectable concentration of these elements in the digestion blank control sample. A significant concentration difference between the slurry sample and blank control sample demonstrates the existence of the corresponding element in the slurry sample.

958

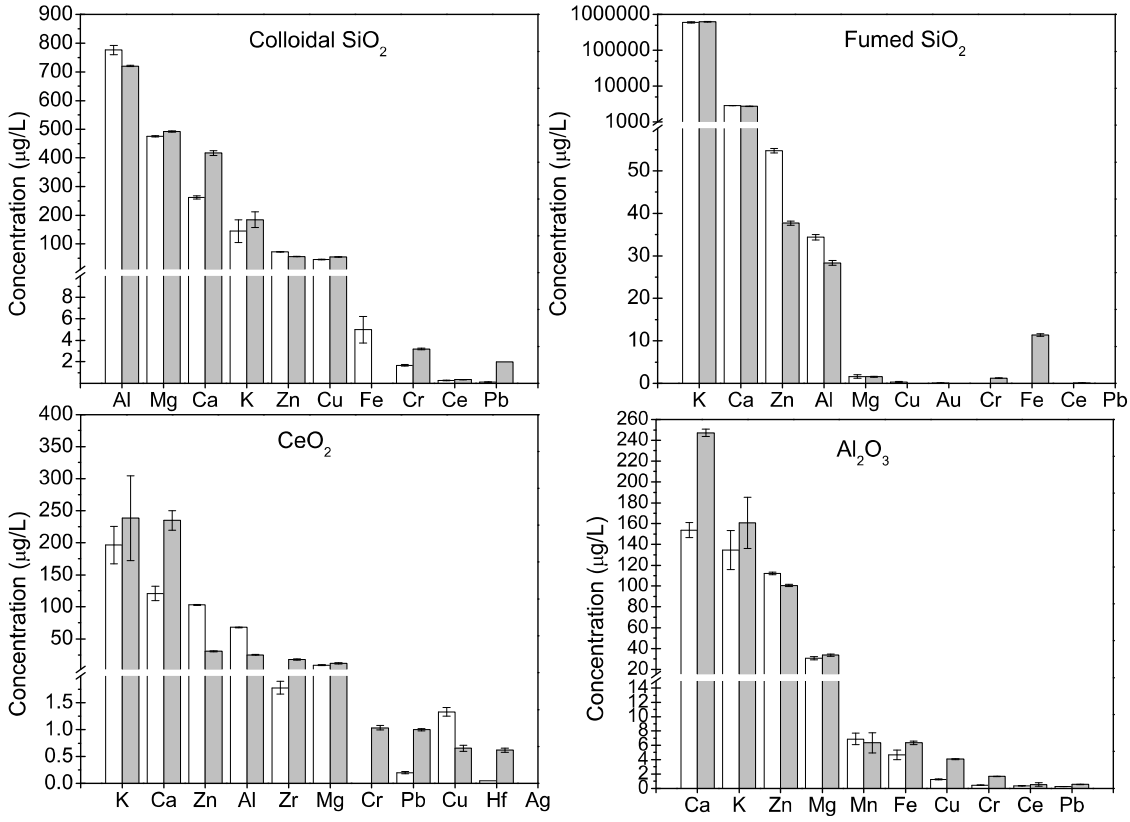

959

960 **Fig. 3**. Concentration of elements other than the major metals (Si, Ce or Al) in the liquid phase
961 of four CMP slurries. Open bars represent liquid sample prepared by centrifugal ultrafiltration;
962 solid bar represent liquid sample prepared by high speed centrifugation.

963

964

965

966

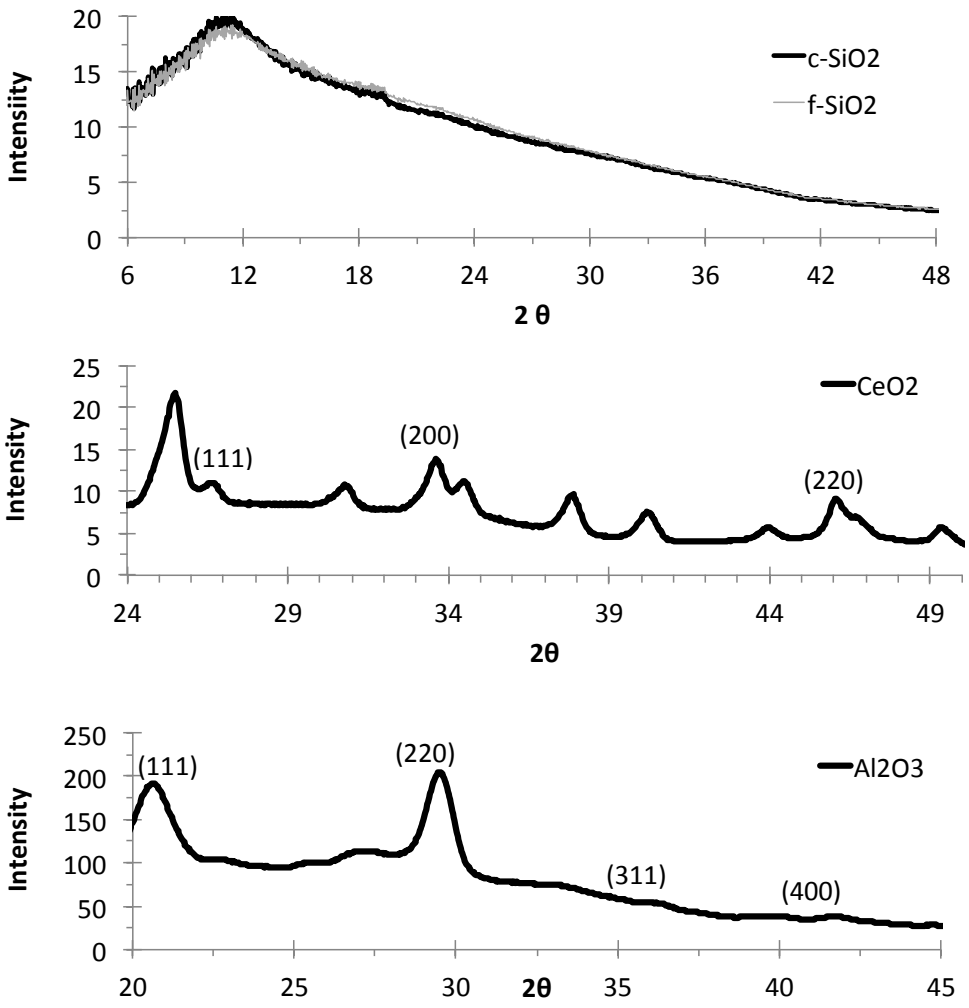

967

968

969

970 **Fig. 4**. X-ray diffraction pattern of SiO_2, CeO_2, and Al_2O_3 slurries after drying.

971

972

973

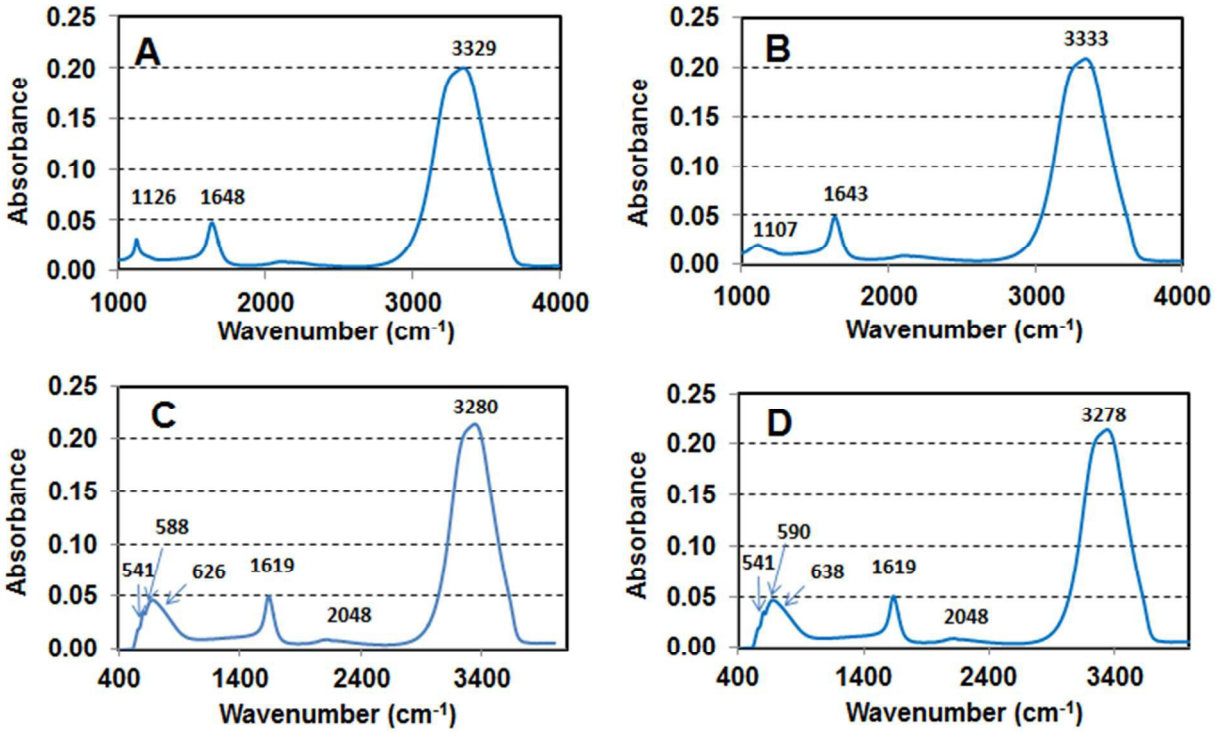

974

975

976 **Fig. 5**. FT-IR spectra of *c*-SiO_2 (A), *f*-SiO_2 (B), CeO_2 (C), and Al_2O_3 (D) slurries.

977

978

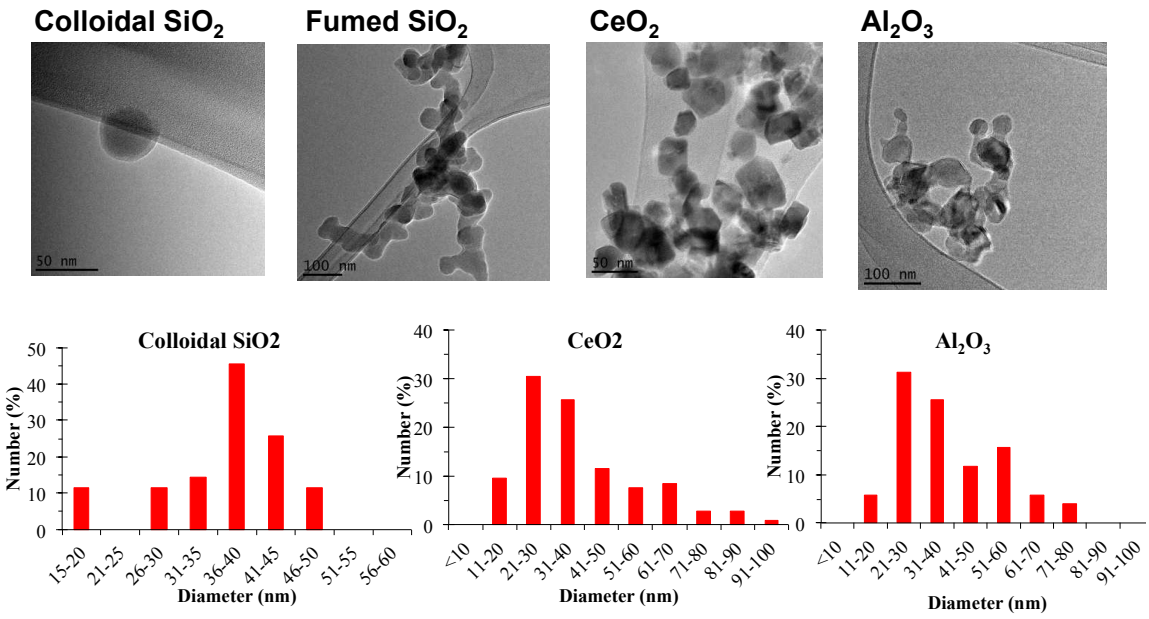

979

980

981 **Fig. 6**. TEM images and TEM based particle size distributions for CMP nanoparticles. The size

982 distribution histogram for colloidal silica, ceria, or alumina is obtained by sizing > 50 particles

983 under the corresponding TEM images. Fumed silica particles were not sized because of their

984 coalesced state.

985

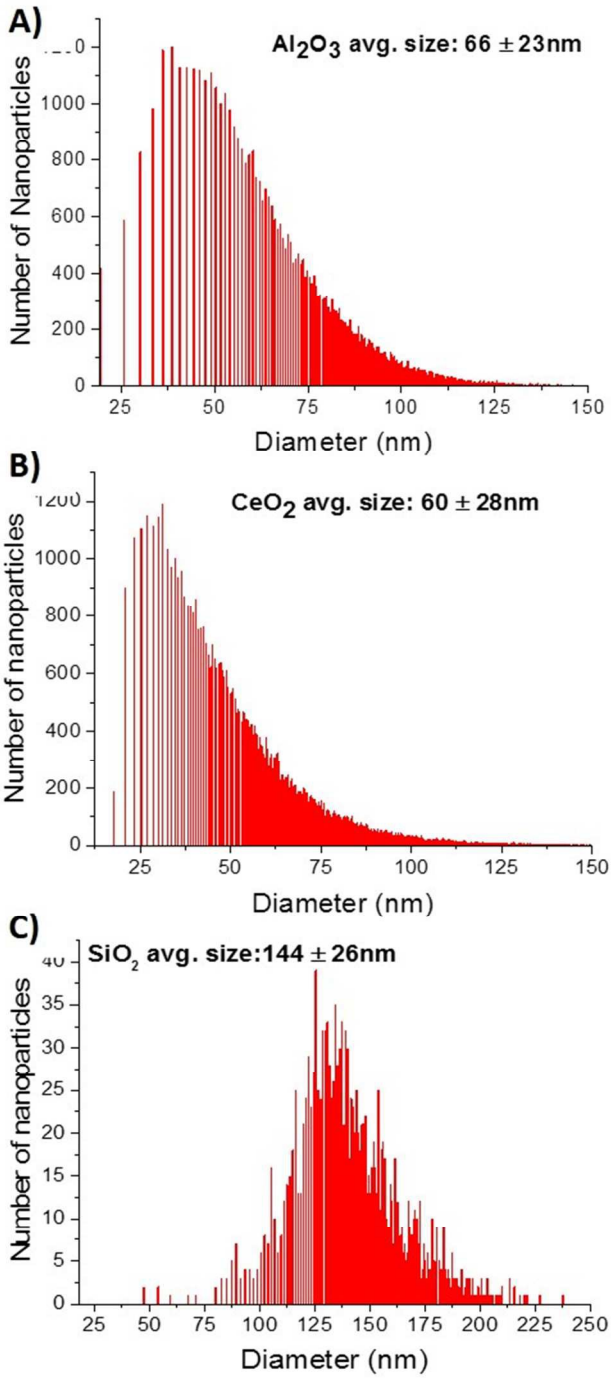

986

987 **Fig. 7.** Size distributions of Al_2O_3 (A), CeO_2, (B), and *f*-SiO_2 (C) CMP slurries by single particle

988 ICP-MS.

989

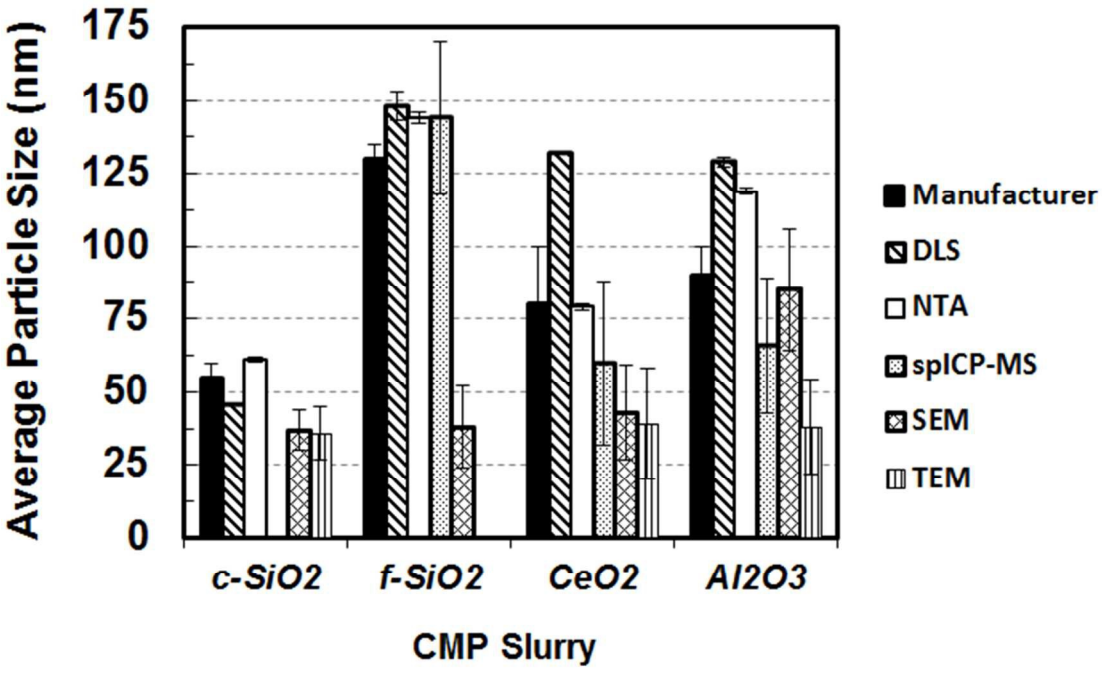

990

991

992 **Fig. 8**. Comparison of the average particle size values determined in this study for the various

993 CMP slurries using different techniques with values reported by the slurry manufacturer.

994
995

996

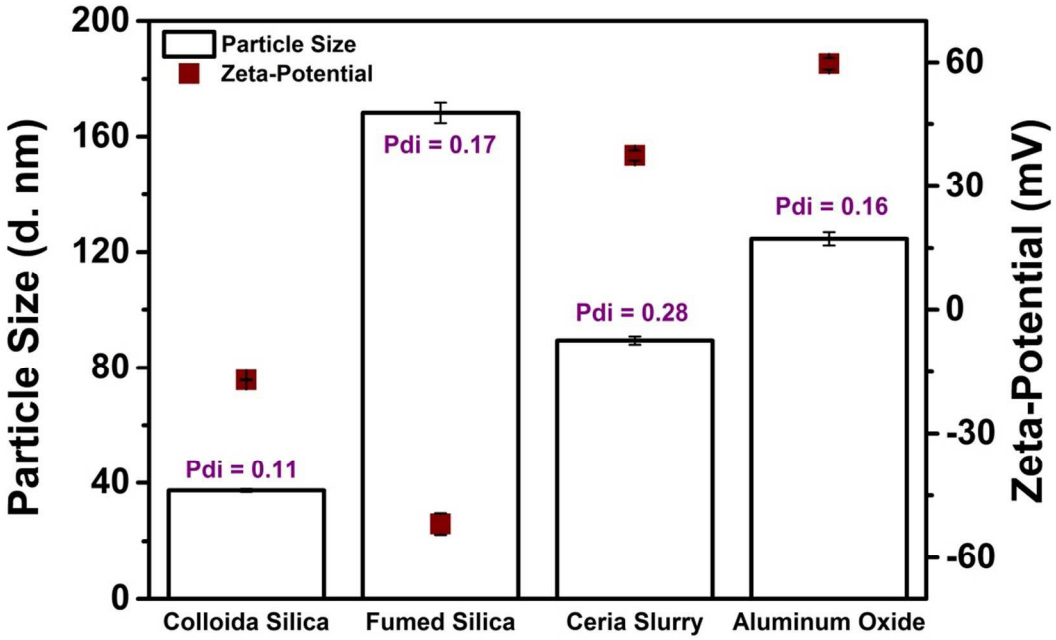

997

998

999 **Fig. 9**. Dynamic light scattering (bars) and zeta potential analysis (squares) of CMP slurries

1000 (ambient slurry pH). Polydispersity index (Pdi) values are shown for DLS data.

1001
1002

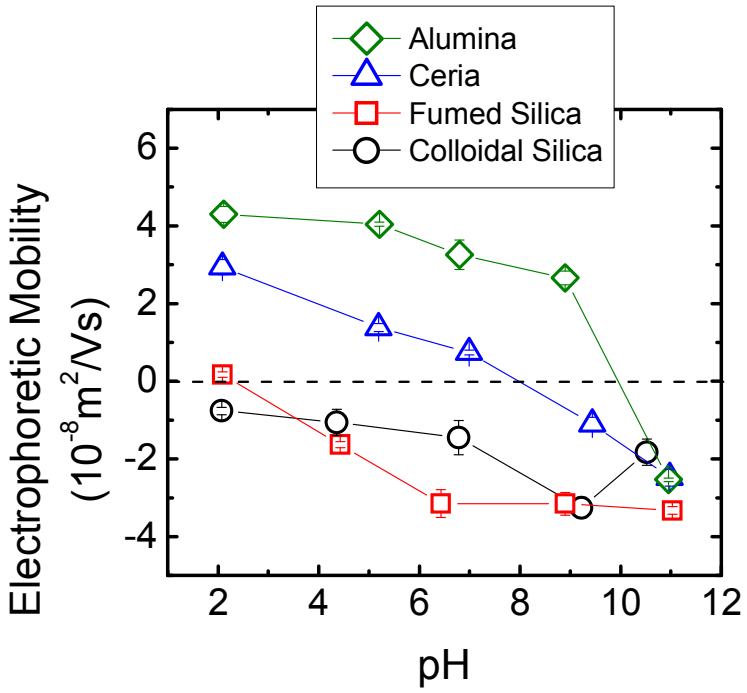

Fig. 10. EPMs of four CMP nanoparticles in 1 mM NaCl solutions prepared at different pH conditions. The error bars represent the standard deviation of triplicates.

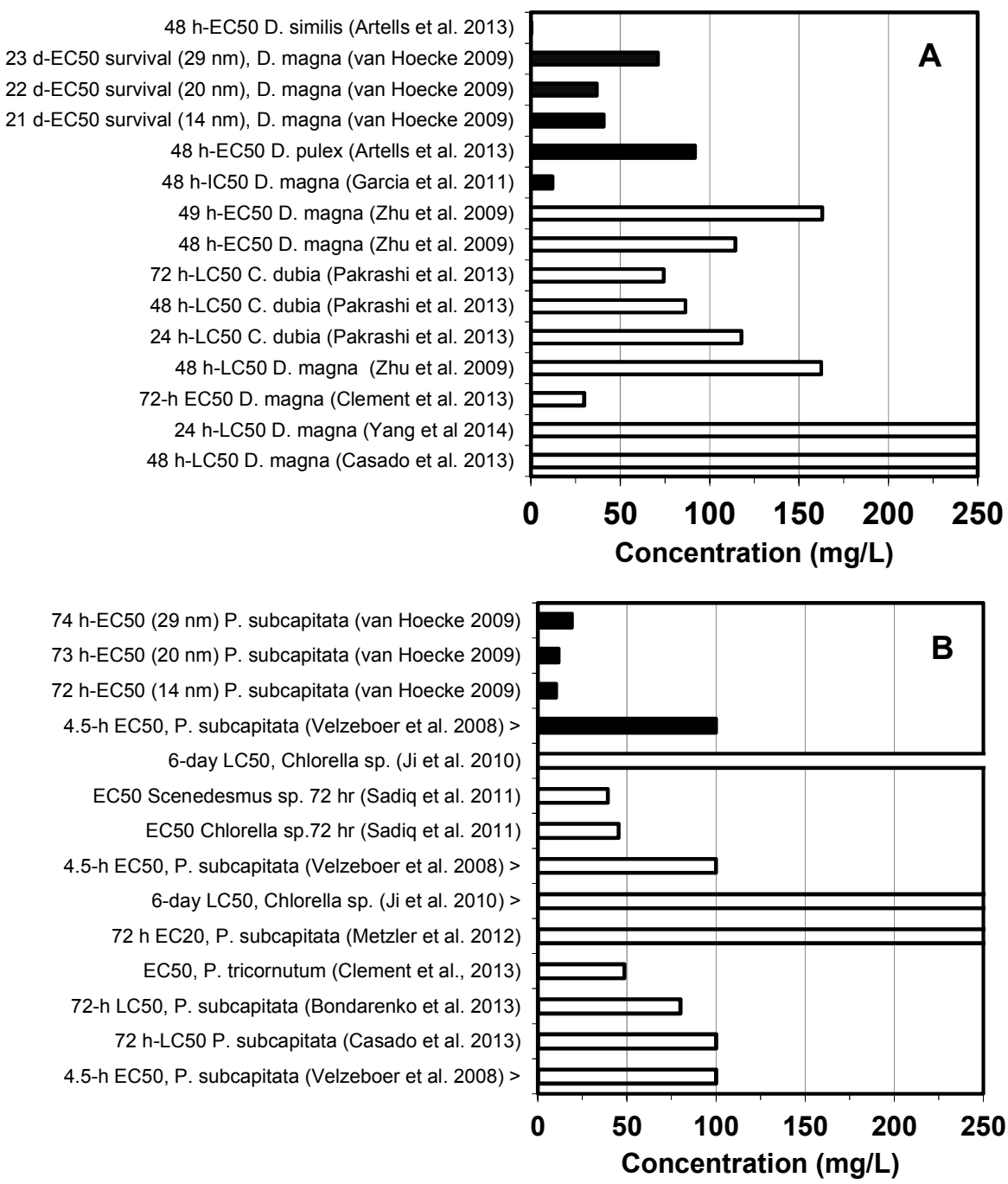

Figs. 11A and 11B. Ecotoxicity findings determined in bioassays with freshwater crustaceans (*Cladocera*) (**A**) and algae (**B**) for three major classes of metal-based nanoparticles used in CMP slurries. Note: *D. similis= Daphnia similis; D. magna= Daphnia magna; D. pulex= Daphnia pulex; C. dubia= Cerodaphnia dubia; P. subcapitata= Pseudokirchneriella subcapitata.* . Legends: Data for CeO_2 (■), Al_2O_3 (□), and SiO_2 (▨).

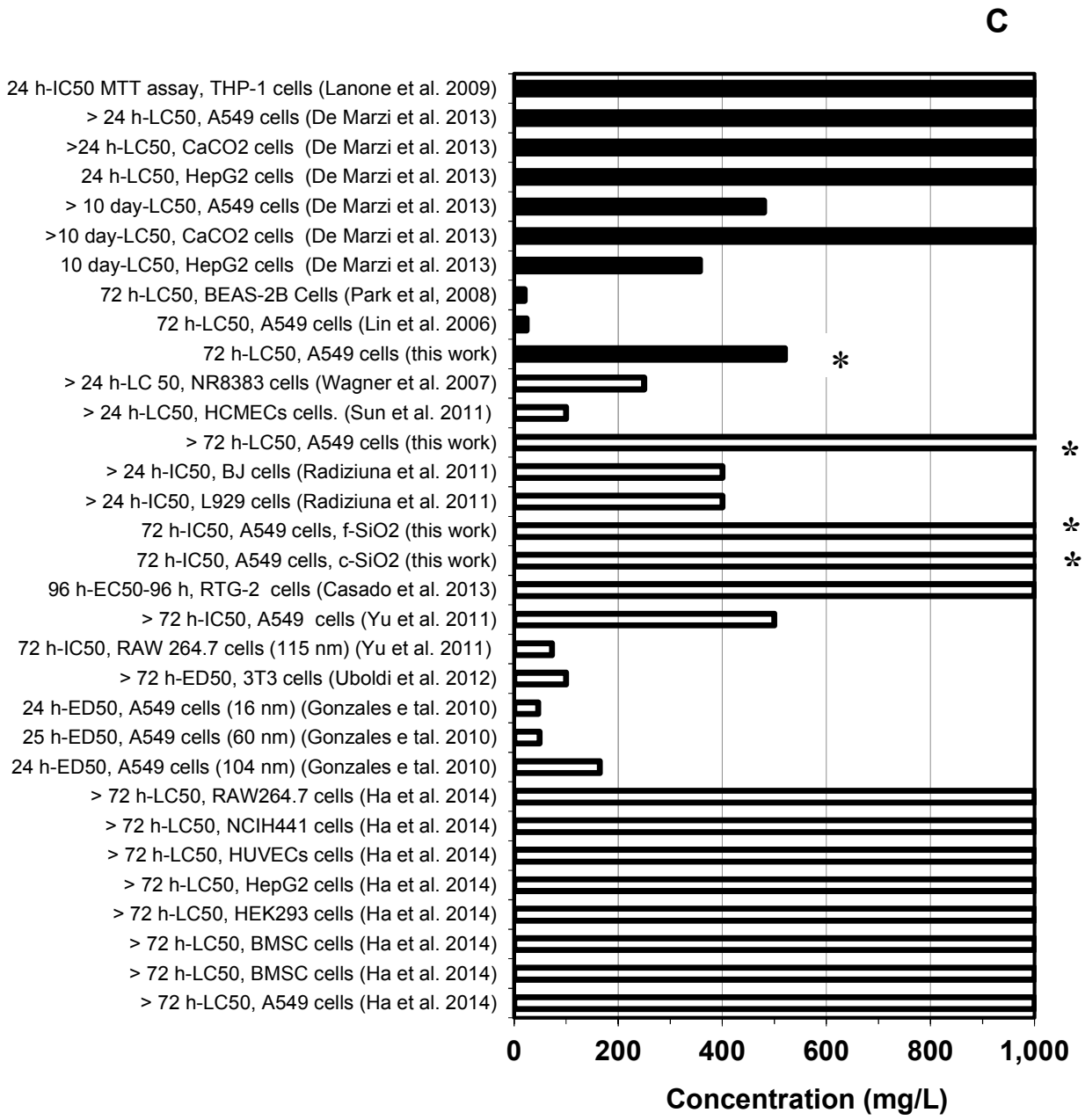

Fig. 12. Human cytotoxicity findings for three major classes of metal-based nanoparticles used in CMP slurries. Legends: Data for CeO_2 (■), Al_2O_3 (□), and SiO_2 (▨).The asterisk (*) indicates data obtained in this study.

Nano Impact Statement

The manuscript represents the efforts of an academic-industry consortium aiming to characterize the physical-chemical and biological attributes of a major class of engineered nanomaterials (CMP slurries). Results include intra-laboratory comparisons of measurements, multiple independent measurements of particle sizes and multiple, complimentary assays to assess human cell and bacterial response to nanomaterials. The results are compared with other reported measurements, and put into a life cycle perspective that aims to understand both exposure and hazards. The conclusion is that CMP nanoparticles pose relatively low risk based upon our current understanding, but that biological effect differences between fumed and colloidal silica continue to be unresolved when considering the available physical chemical data.